Deformed Pleistocene marine terraces along the Ionian sea margin of southern Italy: Unveiling blind fault-related folds contribution to coastal uplift.

Enrico Santoro[1], Luigi Ferranti[1], Pierfrancesco Burrato[2], Maria Enrica Mazzella[1], and Carmelo Monaco[3]

[1]Dipartimento di Scienze della Terra, Università di Napoli “Federico II”, Largo S. Marcellino 10, 80138, Napoli, Italy.

[2]Istituto Nazionale di Geofisica e Vulcanologia, Via di Vigna Murata 605, 00143, Roma, Italy.

[3]Dipartimento di Scienze Geologiche, Università di Catania, Corso Italia 55, 95129, Catania, Italy.

Morphotectonic analysis and fault numeric modeling of uplifted marine terraces along the Ionian Sea coast of the Southern Apennines allowed us to place quantitative constraints on Middle Pleistocene-Holocene deformation. Ten terrace orders uplifted to as much as +660 m were mapped along ~80 km of the Taranto Gulf coastline. The shorelines document both a regional and a local, fault-induced contribution to uplift. The intermingling between the two deformation sources is attested by three 10 km-scale undulations superimposed on a 100-km scale northeastward tilt. The undulations spatially coincide with the trace of NW-SE striking transpressional faults that affected the coastal range during the Early Pleistocene. To test whether fault activity continued to the present, we modeled the differential uplift of marine terraces as progressive elastic displacement above blind oblique-thrust ramps seated beneath the coast. Through an iterative and mathematically based procedure we defined the best geometric and kinematic fault parameters as well as the number and position of fault segments. Fault numerical models predict two fault-propagation folds cored by blind thrusts with slip rates ranging from 0.5 to 0.7 mm/a and capable of generating an earthquake with a maximum moment magnitude of 5.9-6.3. Notably, we find that the locus of predominant activity has repeatedly shifted between the two fault systems during time, and that slip rates on each fault have temporally changed. It is not clear if the active deformation is seismogenic or dominated by aseismic creep; however, the modeled faults are embedded in an offshore transpressional belt that may have sourced historical earthquakes.

1. Introduction

It is widely acknowledged that morphotectonic analysis constitutes a fundamental ingredient of active tectonic studies. Particularly, displaced marine terraces are used to unravel uplift rate histories and fault-induced landscape deformations at active coastal settings [e.g. *Valensise and Ward*, 1991; *Ward and Valensise*, 1996; *Cucci and Cinti*, 1998; *Dubar et al.*, 2008; *Ferranti et al.*, 2009; *Gaki-Papanastassiou et al.*, 2009; *Caputo et al.*, 2010; *Berryman et al.*, 2011; *Saillard et al.*, 2011]. A paleo-shoreline shape differing from the original horizontal attitude which formed at the coeval sea-level reflects deformation which may have been driven by large-scale and deep-seated geodynamic sources, by local processes occurring at shallower depths (e.g. fault slip and fold growth), or by a combination of both [e.g. *Ferranti et al.,* 2009; *Caputo et al.*, 2010]. If, within the shoreline deformation profile, the regional and local tectonic components can be separated, the possibility is offered to better constrain the geometric and kinematics parameters of faults, which cannot otherwise be investigated with conventional paleoseismic methods.

A suitable setting where these notions can be tested is represented by the Apennines orogen in southern Italy, where recent coastal markers are ostensibly deformed [*Caputo and Bianca*, 2005; *Ferranti et al*., 2006; *Antonioli et al*., 2009]. At the end of the Early Pleistocene, a major tectonic change occurred in southern Italy [*Hippolyte et al*., 1994]. At this time, east-directed motion of the Apennines frontal thrust system became locked, probably because of involvement of the foreland continental lithosphere in the Adriatic subduction zone. This occurrence caused in turn the activation of NW-SE striking transpressional faults along the Ionian Sea margin of the Apennines (Figure 1), which served to accommodate further albeit slow convergence between the Adriatic foreland and the Apennines [*Catalano et al*., 1993]. The transpressional structures were coeval with extensional faults in the west (Figure 1), which are linked to back-arc thinning in the Tyrrhenian Sea at the rear of the Apennines (Section 1 in Figure 1) [*Hippolyte et al*., 1994]. Around the same time, generalized uplift of the southernmost part of the Apennines and the Calabrian Arc commenced (Section 1 in Figure 1) [*Westaway*, 1993].

Whereas the extensional faults are relatively well exposed and are the sources of instrumental and destructive historical earthquakes (DISS Working Group, 2010, Database of Individual Seismogenic Sources, Version 3.1.1, available from INGV, http://diss.rm.ingv.it/diss/), post-Early Pleistocene deformation in the eastern side of southern Italy is, however, difficult to assess. Because the frontal sector of the Apennines experienced a recent tectonic reorganization and has relatively low deformation rates and seismic activity [e.g. *Chiarabba et al.,* 2005; 2008; *D'Agostino et al.,* 2008; *Devoti et al.*, 2008; *Ferranti et al.*, 2008], several limitations are encountered when trying to unravel the recent deformation pattern. Geomorphic markers like marine terraces, being long-lived topographic feature capable of integrating slow deformation over long periods of time, can be used as paleogeodetic indicators to solve this problem.

Previous studies on uplifted marine terraces along the Taranto Gulf, a major embayment of the Ionian sea (Sections 1 and 2 in Figure 1), interpreted local paleo-shorelines deformations superimposed on the regional uplift signal in the central part of the Gulf as due to fault-propagation folds linked to deep contractional structures [*Ferranti et al.*, 2009; *Caputo et al.*, 2010]. In the last decades, the increasing density of seismometer networks has allowed detailed study of earthquakes that occur along buried contractional faults (e.g. El Asnam, Algeria, 1980, Mw = 7.3 [*Yielding et al.*, 1981]; Coalinga, California, 1983, M = 6.5 [*Stein and King*, 1984]; Kettleman Hills, California, 1985, M = 6.1 [*Ekström et al.*, 1992]; Los Angeles Basin California, 1987, M = 6.0 [*Hauksson and Jones*, 1989]; Spitak, Armenia, 1988, M = 6.8 [*Kikuchi et al.*, 1993]; Chi-Chi, Taiwan, 1999, Mw = 7.5 [*Yu et al.*, 2001]). With the exception of the Chi-Chi earthquake, these events show a progressive decrease of the dislocation from the hypocenter toward the surface, which is only characterized by small fractures or secondary faulting (e.g. extensional faults associated with the bending moment).

The investigation of subtle superficial deformation related to these structures through a morphometric analysis may return basic but robust information on the geometry and kinematics of otherwise invisible faults. The morphometric analysis is customarily blended with fault numeric modeling in order to place constraints on geometry, kinematics and slip rates of blind faults [*Rockwell et al.*, 1988; *Valensise and Ward*, 1991; *Ward and Valensise*, 1996; *Keller et al.*, 1998; *Benedetti et al.*, 2000; *Ponza et al.*, 2010]. The underlying idea is to iteratively compare the geometry of a deformed zone, reconstructed by means of geomorphic markers, with the spatial distribution of surface displacements evaluated through fault numeric modeling.

In this study, we focused on the uplifted marine terraces preserved along the southern half of the Taranto Gulf between the Sibari Plain and the southern border of the San Nicola Plain, where previous work proposed the existence of deformation induced by local thrust and transpressional faults (Figure 1). The paleo-shorelines profiles reconstructed from a detailed mapping of the terraces were used to calibrate the geometric and kinematic parameters of active structures deforming the coastal area. In order to shed light on the local deformation contribution, we derived the regional signal by interpolating the uplift pattern derived from MIS 5.5 terrace elevation along the entire Gulf, from Taranto city to the Sila massif (Section 1 in Figure 1). The local tectonic signal in the central part of the Gulf, along the coast of the Pollino mountain range, was interpreted by performing elastic fault numeric modeling of the vertical co-seismic displacement benchmarked on the paleo-shorelines profiles, with the regional signal removed.

The results of our analysis highlight the usefulness of an integrated morphometric and fault modeling approach to investigate subdued landscape deformations and to define geometry, kinematic and temporal behavior of potentially active blind structures. Moreover, the unprecedented resolution of the shoreline terraces has permitted to snapshot with extreme detail how fault activity is spatially and temporally partitioned between fault segments, a vital information to comprehend the mechanism of distributed deformation.

2. Tectonic background

2.1. Regional setting

The Southern Apennines formed during Cenozoic slow relative convergence between Europe and Africa and fast subduction and roll-back of the Adriatic-Ionian slab associated with back-arc stretching in the Tyrrhenian Sea [*Malinverno and Ryan*, 1986; *Faccenna et al*., 2001]. These processes caused the eastward migration, toward the Apulian sector of the Adriatic foreland, of paired contractional and extensional belts [*Patacca et al*.,1990; *Monaco et al*., 1998; *Menardi-Noguera and Rea*, 2000; *Van Dijk et al*., 2000]. Today, regional GPS velocity fields point to a reduction in the rate of slab rollback and Tyrrhenian back-arc extension with respect to geologic rates, and whether subduction is ongoing is still an open question [*Oldow et al.*, 2002; *Hollenstein et al.*, 2003; *D'Agostino and Selvaggi*, 2004; *D'Agostino et al.*, 2008; *Devoti et al.*, 2008]. A Wadati-Benioff zone is well defined only beneath the Calabrian arc south of the Apennines (Section 1 in Figure 1) and is represented by a steep, 200 km long plane that can be followed from the Ionian sea down to a depth of 500 km below the Tyrrhenian Sea [*Selvaggi and Chiarabba*, 1995; *Faccenna et al.*, 2005, 2011; *Chiarabba et al.*, 2008]. The deep northeastern limit of the Ionian subduction is located in northern Calabria, and represents the transition between Apulian continental crust and attenuated or oceanic Ionian crust [*Catalano et al.*, 2001] (Section 1 in Figure 1).

Motion of the thin-skinned thrust front in the Southern Apennines reportedly ceased during Early Pleistocene as the front was buried beneath the western margin of the Bradano foredeep basin [*Patacca and Scandone*, 2001] (Figure 1). In the meantime, involvement of thick Apulian continental crust in the Southern Apennines subduction and the consequent change in local convergence direction caused the activation of transpressional faults breaking through the previously emplaced thin-skinned allochthon (Figure 1) [*Knott and Turco*, 1991; *Catalano et al.*, 1993; *Monaco et al.*, 1998; *Van Dijk et al.*, 2000; *Tansi et al.*, 2007]. Motion of these faults substantially occurred during the Early Pleistocene. On the other hand, morphological analyses have identified that shortening in the frontal zone occurred during more recent time as well [*Caputo and Bianca*, 2005; *Caputo et al.*, 2010], and may still be ongoing [*Ferranti et al.*, 2009].

Current deformation in southern Italy, as indicated by seismicity and geodesy, is however dominated by an extensional fault array along the Apennines axial zone (Figure 1). The extension direction determined by fault slip analyses [*Hippolyte et al.*, 1994; *Monaco and Tortorici*, 2000; *Maschio et al.*, 2005; *Papanikolaou and Roberts*, 2007], focal mechanisms of crustal earthquakes (CMT and RCMT Catalogues) and GPS geodetic velocities [*Hunstad et al.*, 2003; *Ferranti et al.*, 2008] trends ~NE-SW in the Apennines and ~E-W in northern Calabria. The frontal belt of the southern Apennines together with the Calabrian Arc, has experienced sustained uplift (~1 mm/a) since the Middle Pleistocene, that formed flights of marine terraces hundred of meters above the present sea-level [e.g. *Westaway*, 1993; *Miyauchi et al.*, 1994; *Cucci and Cinti*, 1998; *Westaway and Bridgland*, 2007; *Ferranti et al.*, 2009; *Santoro et al.*, 2009; *Caputo et al.*, 2010]. Uplift is viewed as an isostatic [*Westaway*, 1993; *Wortel and Spakman*, 2000; *Gvirtzman and Nur*, 2001] or dynamic response to removal of a high-density deep root, or as a dynamic response to mantle upwelling processes [*Faccenna et al.*, 2011].

A local tectonic component is also embedded in the uplift budget. Small amplitude and wavelength undulations in paleo-shorelines document the superposition of local, fault-induced, deformations on a general northeastward tilt of northern Calabria [*Cucci and Cinti*, 1998; *Ferranti et al.*, 2009; *Caputo et al.*, 2010].

2.2. Tectonic frame of the Ionian margin of the southern Apennines

The mountain belt in northern Calabria and southern Lucania is floored by different tectonostratigraphic units (Figure 1), which were stacked since the Oligocene-Miocene along a roughly NW-SE trending thrust system [*Knott*, 1987; *Cello et al.*, 1989]. The higher units are represented by remnants of an accretionary wedge and their satellite basin cover related to subduction of the Neothetys ocean (Liguride and Sicilide complexes, Figure 1). The lower unit is a deformed stack of Mesozoic basinal rocks and platform carbonates, the latter forming the backbone of the Pollino Range (Figure 1). After Late Miocene, all these units were thrust over the Apulian foreland platform, which was itself involved in thick-skinned thrusting [*Menardi-Noguera and Rea*, 2000]. The youngest units in the investigated area are represented by Pliocene-Middle Pleistocene fan-delta sediments [*Colella*, 1988] filling the Sibari Plain, marine clayey terrigenous deposits (Argille Subapennine Formation), extensively outcropping in San Nicola Plain and laterally correlative of the Bradano foredeep infill, and Middle Pleistocene-Holocene coastal and continental deposits (Figure 1).

The study area lies between the frontal thrust of the belt, buried beneath the Bradano foredeep, and the chain axial sector affected by the active normal faulting (Figure 1). Along the western border of the Sibari Plain, the extensional belt is represented by the Pollino-Castrovillari fault (PCF; Figure 1), a NNW striking, WSW dipping, ~15 km long normal fault, with several scarps cutting through Middle Pleistocene-Holocene continental deposits [*Michetti et al*., 1997; *Cinti et al*., 2002]. Based on geomorphic and paleo-seismological studies [*Cinti et al*., 1995, 1997] this fault is considered active; radiocarbon dating of organic material recovered in paleo-seismological trenches evidenced that the two most recent earthquakes occurred in 2000-410 B.C. and 530 A.D.-900 A.D. [*Cinti et al*., 2002].

No active crustal normal fault is known along the Ionian Sea coast. Instead, *Catalano et al*. [1993] mapped Early-Middle Pleistocene strike-slip faults in this sector of the Southern Apennines. Several WNW-ESE striking left-lateral strike-slip faults were recognized (CF, STF, PF, SRF, VF and CNNF in Figure 1) that, together with ~N-S striking, westward displacing, thrust faults, pushed Apulian carbonate wedges up through the overlaying allochthonous Liguride rocks. Based on seismic reflection profiles and borehole data (Section 1 in Figure 2a), *Del Ben et al*. [2007] and *Ferranti et al*. [2009] suggested that the strike-slip fault zones also controlled the offshore morpho-structural evolution (Figure 2a), where positive flower structures deform up the recent Pleistocene sequences. *Ferranti et al*. [2009], through detailed structural analysis carried on the clayey sequences (Argille Subappennine) outcropping along the coastal area, documented that the strike-slip fault zones were activated with a ~NE to ENE-trending shortening axis (Figure 1) during the Early-Middle Pleistocene.

Instrumental seismicity from the Italian Seismic Catalogue (CSI) is at low level and shows only scattered events in the region, with no recognizable hypocentral trend [*Chiarabba et al*., 2005; *Frepoli et al*., 2011]. Focal solutions of moderate ($3.0<M<5.3$) crustal strike-slip and thrust earthquakes suggest, however, that the area is still interested by transpressional deformation [*Ferranti et al*., 2009] (Section 2 in Figure 1). The P axis of the incremental strain tensor trends from ~NE-SW to ~E-W for both thrust and strike-slip earthquakes (Section 2 in Figure 1), in agreement with the structural data from recent deposits (Figure 1).

Similarly, the historical seismicity record of this region shows small and only occasional moderate events (CPTI11, Catalogo Parametrico dei Terremoti Italiani, version 2011; *Rovida et al*. [2011]) whose sources are still debated.

The uplift process active since Middle Pleistocene is well documented by marine terraces extensively found in the area, ranging in elevation from ~5 to ~650 m a.s.l. [*Bianca and Caputo*, 2003; *Cucci*, 2004; *Cucci and Cinti*, 1998; *Ferranti et al*., 2009; *Santoro et al*., 2009; *Caputo et al.*, 2010]. Based on absolute (Electro Spin Resonance) [*Santoro et al*., 2009] and relative (amino acid racemization) [*Cucci*, 2004] dating, although constrained from only two sites, a terrace mapped between ~100 and ~130 m a.s.l. (T4 in the present paper) was correlated to the Marine Isotopic Stage (MIS) 5.5, aged at ~124 ka. By applying the average uplift rate deduced from the MIS 5.5 marine surface elevation (~1 mm/a), the remaining terraces were indirectly attributed to the Quaternary eustatic highstands, extending the chronology back to MIS 15 (~580 ka) [*Santoro et al*., 2009].

Several authors have pointed out the existence of local paleo-shoreline deformations superimposed on the regional uplift process. *Cucci and Cinti* [1998] and *Cucci* [2004] explained the increase in elevation of terraces along the western border of the Sibari Plain as the consequence of co-seismic footwall uplift of the Pollino-Castrovillari normal fault. Based on geomorphic, structural and geophysical data, *Ferranti et al*. [2009] argued that the paleo-shorelines undulations along the Pollino Range were related to Middle Pleistocene-Holocene activity of blind thrusts linked to transpressional shear zones. Finally, *Caputo et al*. [2010] interpreted the increase of uplift and tilting rate moving southward from the Apulia foreland toward the Pollino Range as due to the combination of re-activated out-of-sequence blind thrusts of the Valsinni fault (Figure 1) and deep-crustal shortening.

The terraces are locally affected by deep-seated slope gravitational deformation (DSSGD in Figure 1) [*Varnes et al.*, 1989] triggered by differential uplift and eastward coastal tilting [*Bentivenga et al.*, 2004; *Ferranti et al.*, 2009; *Caputo et al.*, 2010]. These gravitational phenomena formed several not-eustatic terraces that have contributed to foster different interpretations, within published papers, regarding the number of terrace orders, chronological attribution and uplift rates.

3. Uplifted marine terraces

3.1. Terrace mapping and paleo-shorelines reconstruction

Marine terraces were mapped along the coast between the Sibari and San Nicola plains, which bound the Pollino Range to the South and North, respectively. The observations discussed here build on, and refine, the works published by *Ferranti et al*. [2009] and *Santoro et al*. [2009], by slightly adjusting their marine terrace positions based on additional observations, and by extending their terrace map to the southern sector of the San Nicola Plain. In the overlapping area, some terraces position and lateral correlation errors were identified and corrected during the new field analysis presented here.

Ten terrace orders, labeled from T0 to T9 (lowest to highest) were distinguished between ~5 and ~660 m a.s.l. (Figure 2a). Higher remnants were noticed, but due to the very scattered distribution and difficulty in correlation, they were discarded from further analysis.

A lateral correlation of individual terrace remnants was attempted through aereophotography analysis (1:17.000 scale) and field surveys (1:10.000 and 1:5.000 scale topo maps and orthophotos, respectively). Geomorphic correlations (Table 1) were performed considering the altimetric distribution of inner margins (intersection line between abrasion platform and landward sea-cliff), the abrasion platform width (planimetric distance between inner and outer margins) and slope , and the platform-cliff ratio (ratio between width of the terrace and height of the on-looking cliff) [*Verma*, 1973]. Data listed in Table 1 are corrected for the younger colluvial cover on the terraces.

The morphologic parameters of terraces vary along the surveyed coastal sector (Table 1 and Figure 2a). Typically, the terraces are characterized by an increase in width and platform-cliff ratio and by a decrease in platform slope moving southward and northward from the Pollino Range toward the Sibari and San Nicola plains, respectively. This morphologic heterogeneity chiefly arises from a laterally uneven coastal morphology and from the different mechanical properties of the outcropping lithologies [*Amato et al*., 1997]. Indeed, along the Sibari and San Nicola coastal stretches, the abrasion processes active during high stands of protracted duration developed more extensive platforms due to the easily erodible Pliocene-Pleistocene clay and sands underlying the marine terraces. On the other hand, along the Pollino slope the steeper coast and the outcrop of more resistant Miocene and Mesozoic rocks of the accretionary wedge (Figure 1) inhibited the modeling of wide platforms.

In addition, as a consequence of the lower uplift rates in the San Nicola Plain (see the northward decrease in inner margin elevations in Table 1), the increase in platform width and the lesser number of uplifted marine terraces (Figure 2b and Table 1) point to the re-occupation of a platform during successive interglacial transgressions. Particularly, proceeding northward, T2 and T4 loose a clear geomorphologic expression and are reduced to subtle morphologic steps on the surface of higher terraces (T5 and T3, respectively; Figure 2b).

Correlation accuracy between terrace remnants was enhanced through a detailed sedimentological analysis of the terraced deposit, each generally characterized by a transgressive-regressive cycle. Correlation between separate exposures of the coastal deposit hosted by the terraces, which in fortunate cases are found along river valley sides, was used to construct semi-quantitative cross section of the depositional sequences and to define the sedimentary parameters characterizing each terrace order (for a full facies analysis of the deposit see *Santoro et al*. [2009]).

Sedimentological analysis of the terraced deposits was instrumental to determine the position of the terrace inner margin and thus the paleo-shorelines elevation. Commonly, inner margins are considered as the best indicator of the highest position reached by the sea during the eustatic highstand which modeled the terrace. In this work, we considered the highest elevation reached by foreshore deposits in the coastal depositional sequence as the maximum highstand sea level. However, the paleo-sea level position can be modified or obscured by post-emergence erosive and depositional (colluvial and/or alluvial) processes. For each terrace, the estimation of continental cover thickness, as well as the occurrence and the amount of erosion of the primary coastal deposit was estimated on a site-by-site basis, using natural cuts or boreholes [details in *Santoro et al.*, 2009].

Along some parts of the coast, the development of deep-seated slope gravitational deformations (DSSGDs in Figure 1) acts against uplift and obscures a truthful reconstruction of the paleoshoreline pattern [*Ferranti et al.*, 2009]. For this reason, terraces related to the DSSGDs were discarded in the paleo-shoreline reconstruction.

In Figure 3, data points indicate sites where inner margin elevation was measured, with error bars representing the estimated uncertainty derived from a combination of accuracy in marker identification and precision in measurement. The maps used to trace markers have 10-m and locally 5-m contours. Thus, uncertainty in elevation estimates is probably within ±5 m. GPS and altimeters used to retrieve spot locations of inner margins and of other markers have a similar ±5 m uncertainty. The largest error in nominal paleo-shoreline elevation stems from the choice of the appropriate bathymetric correction for different markers (constructional, erosional), which must be evaluated at individual locations. Assigned paleo-bathymetric uncertainty is: ±2 m, where a complete reconstruction of the foreshore depositional sequence associated to individual terraces was possible; ±5 m, where coastal sequences are partially exposed; ±10 m, where the terraced deposits are completely eroded but the shoreline angle can be derived from the platform projection; +20 m where no relation between platforms and their shoreline angle can be established. Error bars attached to data points incorporate both measurement errors and paleo-bathymetric uncertainty.

The paleo-shoreline elevations have been projected along section A-B parallel to the present and ancient coastline (Figure 2a). As noted previously [*Ferranti et al.*, 2009; *Santoro et al.*, 2009], the paleo-shorelines show the superposition of local deformations on the regional uplift process. Three major undulations of maximum ~20 km wavelength and up to ~200 m amplitude are localized along the northern and southern flanks of the Pollino Range and beneath the Sibari Plain (labeled as 1, 2 and 3, respectively, in Figures 2a and 3). As shown in Figure 3, high densities of observation points in the central and northern sector are available and provide a tight constrain on the deformed shape of the coastline. Higher position uncertainties exist in the southern sector due to the erosional removal of older terraces and to the cover of lower orders by Late Quaternary continental deposits filling the Sibari Plain.

3.2. Terrace chronology

The terrace chronology presented in Table 2 is based on a critical review of all the available dating in the Taranto Gulf. Along the southern part of the Gulf, in the coastal area extending from the San Nicola Plain to the Sila massif, the absence of the characteristic Last Interglacial faunal assemblages (*Senegalese Fauna* and, particularly, the *Persististrombus latus* [*Gmelin*, 1971]) have enhanced the application of different absolute and relative dating methods in order to shed light on the terraces chronology [*Brükner*, 1980; *Dai Pra and Hearty,* 1988; *Amato et al*., 1997; *Cucci*, 2004; *Zander et al*., 2006; *Santoro et al*., 2009; *Caputo et al*., 2010]. Unfortunately, agreement among authors dealing with this problem is still lacking. The existing interpretation conflicts chiefly arise from the choice of a proper calibration of the racemization extent of amino acids from mollusk shells. The chronological scheme we present in this section is based on the dates we consider more reliable, as briefly summarized below. More technical aspects and our reasons for discarding other available dates are discussed in Appendix A.

Two different aminozone schemes were proposed for the Taranto Gulf area by *Hearty et al*. [1986] and *Belluomini et al*. [2002]. Ostensible differences exist between the two reported aminozone schemes and are one of the elements that enhanced substantially different marine terrace chronological interpretations in the region [*Amato et al*., 1997; *Santoro et al*., 2009; *Caputo et al*., 2010]. For the interpretation of the racemization data available in the study area we rely on the *Hearty et al*. [1986] Mediterranean aminozone scheme because of the following reasons: 1. it is based on 389 amino acid racemization analysis in the Mediterranean area, firmly calibrated against 7 *Cladocora caespitosa* U/Th ages ; 2. it is in agreement with global isoleucine epimerization data relative to the Last Interglacial [*Murray-Wallace*, 1995]. Conversely, *Belluomini et al*. [2002] calibrated their aminozones with U/Th ages on mollusk shells that can suffer substantial age underestimation problems due to open radiometric system condition during diagenetic processes [*Kaufman et al*., 1971; *McLaren and Rowe*, 1996]. Besides, *Belluomini et al*. [2002] results disagree both with racemization data from Mediterranean sites where chronology is tightly constrained, and with global isoleucine data [*Murray-Wallace*, 1995].

In the northern part of the S. Nicola Plain, between Basento and Cavone rivers, *Brükner* [1980] applied U-series dating technique on two mollusk samples collected from our terrace T2 (site BR80 in Figure 2b). He obtained an age of 75±7 ka from the base of the terrace and one of 63±3 ka at the top of the coastal regressive system. Based on these ages and on paleontological evidences he attributed this terrace (named as T1 in *Brükner* [1980]) to the MIS 5.1.

Along the southern border of the San Nicola Plain, between the Canna and San Nicola rivers, *Dai Pra and Hearty* [1988] evaluated the leucine epimerization in 7 *Glycymeris* samples collected at the outer margin of our terrace T3 (43 m a.s.l.; site DP88 in Figure 2b). They obtained a D-alloisoleucine L-isoleucine ratio (alle/ille ratio) of 0.29±0.02 which they interpreted as suggestive of a MIS 5.3/5.1 age.

Because the age of T2 is constrained in the northern part of the plain by *Brükner* [1980] U-series dating, we attribute the data from site DP88 from the overlying terrace T3 in the southern part of the plain to MIS 5.3 (Table 2).

To the south, approaching the border of the Pollino range, *Amato et al*. [1997] estimated the alle/ille ratios on 3 *Glycymeris* specimens sampled at 102 m a.s.l. on their terrace IV (site AM97-2 in Figure 2b). On the basis of an alle/ille ratio of 0.34±0.01 and of geomorphological and geochronological considerations they correlate, according to *Hearty et al*. [1986], their terrace IV to the MIS 5.5. The detailed location of this sample is questioned by our field mapping. We did not find evidence of the small remnant of terrace IV that *Amato et al*. [1997] mapped just few meters above our terrace T4 (Figure 2b). Instead, we retain that the *Glycymeris* sp. sampled at site AM97-2 (102 m a.s.l.) comes from the uppermost onlaps of T4 beach deposits above the coeval sea-cliff. Notwithstanding the small discrepancy, the dating result of *Amato et al*. [1997] allows attributing terrace T4 to the MIS 5.5, in agreement with the ages discussed above for the lower terraces in the north.

The attribution of T4 to the Last Interglacial is supported by chronological constraints in the southern Taranto Gulf. *Santoro et al*. [2009] reported an ESR age of 135±20 ka for a *Cardium* sp. collected from T4 close to Vaccarizzo Albanese village on the northern slope of the Sila Massif (site SA09, Figure 1), which permitted to correlate T4 with the MIS 5.5. This age is in agreement with the work of *Cucci* [2004], who evaluated the racemization (D/L ratio) in aspartic acid from 4 in-situ *Glycymeris* sp. collected from terrace T4 close to Trebisacce village, on the eastern slope of the Pollino Range (site CU04 in Figure 2a). He obtained a good reproducibility among the samples and a D/L ratio of 0.73±0.041 with a predicted age of 130 ka. Because the aspartic acid has a faster racemization rate than leucine [*Wehmiller et al*., 2010], this D/L ratio cannot be interpreted based on the *Hearty et al*. [1986] aminozone scheme and the predicted age was, presumably, obtained indirectly through statistical and kinetic racemization models [e.g. *Wehmiller et al*., 2010; *Hearty*, pers. com. 2012; *Cucci*, pers. com., 2012].

Terraces T1, T5, T6, T7, T8 and T9 were indirectly dated by applying the mean uplift rate evaluated from T2, T3 and T4 inner margin elevations to theoretical terraces formed in correspondence with eustatic interglacials of the *Waelbroeck et al*. [2002] sea-level curve and *Lisiecki and Raymo* [2005] $\delta^{18}O$ curve. The mean uplift rate was evaluated at the SW border of the Sibari Plain and at the San Nicola Plain, away from the major shoreline undulations (Figure 3). Comparing this theoretical values with our paleo-shoreline elevations we obtained the following correlations: T1 (MIS 3.5), T5 (MIS 7.1), T6 (MIS 7.5), T7 (MIS 9.5), T8 (MIS 11) and T9 (MIS 15.1). All the terraces but T1 are correlated with highstands during interglacials when the glacio-hydro-isostatic condition was very similar to the present-day Holocene transgression. As a result, we are confident about the correlation accuracy. For the terrace T1, which corresponds to an highstand during an interstadial, we acknowledge that a greater uncertainty, related to unknown glacio-hydro-isostatic effects, is embedded in our indirect dating.

For the lowest terrace (T0), by using the mean uplift rate value along the southern Pollino coast, we found that the best age correlation was with MIS 1. In order to estimate accurate age and related paleo-sea level for T0, we used the sea-level curve of *Lambeck et al*. [2011], that takes into account the isostatic response of the crust to the removal of glacial masses both in the northern hemisphere and in the Alps, and to the load of the released water column on the continental shelf in the Taranto Gulf. We considered T0 formation was possible when, during the Holocene transgression, sea-level rise and uplift rates were comparable. The predicted age for T0 is ~6 ka (Table 2).

4. Quantitative estimate of regional and local source contribution to uplift

A first step toward determining the fault-induced signal and derive fault parameters from the paleo-shorelines record requires splitting the total uplift of individual terraces in its regional and local tectonic component. The two components, local and regional, are characterized by different wavelength, which varies from the few 10s to 100 km, respectively, and their understanding requires assessment of different spatial distribution of markers.

Because the regional uplift signal is driven by deep crustal or mantle sources (*Westaway*, 1993; *Ferranti et al.,* 2006; 2010; *Faccenna et al.,* 2011), its large wavelength geomorphological signature was reconstructed by using the elevation of the MIS 5.5 terrace along a ~300 km long coastal sector of the Taranto Gulf (Section 2 in Figure 1 and Section 1 in Figure 4).

Specifically, we used MIS 5.5 elevation data from sectors where the paleo-shorelines are not appreciably deformed by local sources, and namely from the northernmost Taranto Gulf [*Ferranti et al*., 2006], the Sila Massif [*Santoro et al*., 2009] and the San Nicola Plain (this work) (Figure 1 and Section 2 in Figure 1; Table 3). The elevation of the MIS 5.5 terrace in the northernmost Taranto Gulf is well constrained based on the huge amount of available geomorphology, stratigraphy, and paleontology observations [e.g. *Gignoux*, 1913; *Gigout*, 1960a, 1960b, 1960c; *Cotecchia et al*., 1969] and geochronology data [*Dai Pra and Stearns*, 1977; *Hearty and Dai Pra*, 1985; *Belluomini et al*., 2002] (see Appendix A for further details). From the northernmost Taranto Gulf, the elevation of the MIS 5.5 terrace smoothly increases toward the Apennines to the south [*Ferranti et al*., 2006], suggestive of the lack of local deformation sources.

Regarding the Sila Massif, *Galli et al*. [2010] recognized a local deformation of the MIS 5.5 shoreline that appears to be down-dropped in the hanging-wall of the Rossano-Corigliano Fault (RCF; Figure 1).. According to *Molin et* al. [2004], this evidence indicates a recent reactivation of the RCF as a normal fault. In order to avoid this local deformation signal, we included in our regional analysis only the MIS 5.5 terraces preserved between Corigliano Calabro and Spezzano Albanese villages (Figure 1), outside the RCF deformation zone and where the MIS 5.5 shoreline does not show any evidence of deformation [*Santoro et al*., 2009]. Furthermore, as mentioned above, in this coastal sector the MIS 5.5 coastal marker was recognized through the application of the ESR technique [*Santoro et al*., 2009] (Figure 1). Finally, we discarded data from the coast between the Pollino Range and the San Nicola Plain, which is characterized by two local deformation sources, hereafter named Pollino and Valsinni anticlines (Figures 2a and 3).

The linear regression (R^2=0.979) through the MIS 5.5 elevation data highlights a northeastward tilt of the coast with a mean regional gradient of 0.4 m km^{-1} and a tilt rate (gradient of the coastline divided by the MIS 5.5 age) of $3*10^{-3}$ m km^{-1} ka^{-1} (Section 1 in Figure 4). *Cucci and Cinti* [1998], using only the terraces preserved between the Pollino Range and the San Nicola plains, evaluated a slightly higher tilt rate (4.5-$6.0*10^{-3}$ m km^{-1} ka^{-1}). As noted above, this discrepancy likely arises from incorporation of local-source uplift in their estimation (Figures 2a and 3).

The accuracy of our regional uplift trend was verified by plotting it against the observed T4 (MIS 5.5) paleo-shoreline elevation between the Pollino Range and the San Nicola Plain (Section 2 in Figure 4). Indeed, if we force the regional curve to pass close to the tilted (but not folded) terraces of San Nicola Plain, it apparently runs very close by the inflection point between uplift and subsidence for the Pollino and Valsinni anticlines. The inflection point position for the two anticlines was derived using the elastic deformation models of *Okada* [1985] that predict, for a blind thrust with a geometry similar to that of the northern Calabria faults, a co-seismic surface deformation partitioned on the average between an ~84% uplift and ~16% subsidence. It is evident from Section 2 in Figure 4 that the model condition is closely matched by the combined terrace observation data and computed regional trend.

Finally, relying on the assumption that the regional uplift is steady and uniform, we derived regional and local uplift signals for lower and higher terraces. Specifically, we used the MIS 5.5 tilt rate of $3*10^{-3}$ m km^{-1} ka^{-1} to evaluate the regional uplift gradient (MIS 5.5 tilt rate multiplied by Terrace Age; Section 3 in Figure 4) and the local uplift component (elevation difference between the terrace and the regional uplift curve) for individual terrace orders of known or inferred age.

5. Fault modeling

The model built to parameterize the active structures of northern Calabria is based on standard dislocation modeling of slip on buried, rectangular-shaped faults embedded in an elastic half-space [*Okada*, 1985]. Fault location, geometry, dimension and kinematics were constrained from seismic reflection data, fault kinematic analysis, focal mechanisms and through scalar relationships [*Wells and Coppersmith*, 1994]. The numeric models were performed by using the Fault Studio software (a technical report of the version 1.1 is provided by *Basili, R.*, INGV, http://www.earth-prints.org/handle/2122/1039) a MapBasic application which uses a geographical interface and was developed to calculate geometrical and kinematics parameters of seismogenic sources. The best geometric and kinematics parameters were chosen based on iterative comparison between the observed geomorphic markers deformation and displacement models output.

5.1. Fault geometry and kinematics parameters

Geometric parameters for the modeling of transpressive structures at the coast were derived from the interpretation of offshore seismic reflection profiles [*Ferranti et al*., 2009; *Mazzella,* 2011] (Figure 2a). Because of its ~100 km length extending from the Sibari Plain to southern Apulia, and the strike almost orthogonal to the tectonic structures, the F75-89 multichannel seismic reflection profile was chosen as the most representative to investigate the target faults (Figure 5). In order to extract data about dip and minimum depth of the investigated faults the F75-89 seismic profile was depth converted (see Appendix B and *Mazzella* [2011], where full details of methods and results are discussed).

Inspection of the profile indicates that recent deformation is controlled by steep reverse faults (Section 2 in Figure 5) extending down to ~8-10 km depth and locally deforming the Apulian carbonate rocks (Section 1 in Figure 1). At a shallower level, these thrusts displace the Lower Pleistocene clay and apparently fold the overlying sequence up to the sea bottom (Section 2 in Figure 5). The recent activity of these faults is well documented by the growth geometry of the Pliocene-Quaternary succession (Section 2 in Figure 5), characterized by a variable thickness moving from the Amendolara High (~0.5 km) to the Sibari Basin (~3.5 km; Section 2 in Figure 5).

The major morpho-structural feature in the profile is the Amendolara high (Section 2 in Figure 5) that forms a positive structure bounded by SW- (AMF) and NE- (SPBF) verging thrusts. Careful mapping of displaced early Pleistocene reflectors [*Mazzella*, 2011], points to vertical displacement rates ranging from 0.26 to 0.30 mm/a accrued along the AMF and the SPBF, respectively.

Following *Ferranti et al*. [2009], the faults highlighted in the F75-89 profile were laterally correlated to the onshore structures in order to extract fault geometric parameters for modeling (Table 4). Specifically, the AMF is correlated with the PF, the STF, and the SRF, and the SPBF is traced into the VF (Figure 2a; Table 4). Based on the above correlation, the depth converted profile was used to derive dip as well as minimum depths of the modeled fault surfaces, and the relative uncertainty range.

Kinematics parameters (rake) of the modeled transpressive faults rely on structural analysis carried out in recent deposits (Figure 1) [*Ferranti et al*., 2009] and on strain tensor data derived from available focal mechanisms (Section 2 in Figure 1). At the southeastern tip of the STF and SRF, the Early Pleistocene clays are affected by left transpressive faults active with a ~NE- to ENE-trending shortening axis (sites FE09-1 and FE09-2 in Figure 1). South of this site, Middle Pleistocene sands and conglomerates are tilted and cut by meters-scale reverse faults indicating NE-SW shortening (site FE09-3 in Figure 1). Similarly, focal solutions of small to moderate crustal earthquakes have a P axis of the incremental strain tensor trending from ~N-S to ~E-W, with the two events closer to the study area having a NE-SW axis (Section 2 in Figure 1) .

In light of the small scatter in both the finite and incremental shortening trend estimates, we determined the preferred orientation carrying out a set of fault models with different shortening axis trend changing from NNE-SSW to E-W, tested against the MIS 5.5 terrace. We found that the model with a N30°E shortening axis better fits the MIS 5.5 deformation profile. Based on this, we proceeded in the model steps holding fix the fault rake derived by using a N30°E axis orientation and the geometric parameters established from the seismic profile. Without a-priori information, we used for the slip per event an arbitrary value of 1 m.

Finally, for the Pollino-Castrovillari normal fault (PCF) we used the parameters listed in the DISS database (DISS Working Group, 2010) that were derived from the geomorphic and paleoseismological studies of *Cinti et al*. [1995, 1997] (Table 5). *Cinti et al*. [1997] did not find evidence of horizontal movements along the fault, and thus we used for the model a pure dip slip motion (Table 5) and a mean slip per event of 1.2 m.

5.2. Output fault models for the Pollino coastal fault segments

In order to determine the geometry, position and number of fault segments that potentially deform the terraces along the coast of the Pollino Range, we generated several fault models using the range of geometric values reported in Table 4, and iteratively comparing vertical displacement models with paleo-shorelines profiles. In a first step, using the mean geometric parameters derived from the seismic profile F75-89 (Table 4), we modeled all the fault systems that cross the coastal area. We found that only the Satanasso and Valsinni faults (STF and VF, respectively; Section 1 in Figure 6) are involved in warping of the marine terraces. Indeed, the surface deformational areas predicted by the numeric models for CF, PF and CNNF are not geographically coincident with paleo-shorelines dislocation. Therefore, we regard these latter faults as inactive and discard them from further modeling. In a second step we focused our attention on the STF and VF in order to iteratively determine the best geometric parameters as well as the number and the position of fault segments that best account for the paleo-shorelines deformation. Because the fold wavelength is controlled by dip and width of the fault plane, we used our deformed paleo-shorelines (geographic position and distance between anticline and syncline axis) to calibrate the width, maximum depth and dip of the fault surfaces by moving in the value ranges reported in Table 4, with steps of 1 km and 1°, respectively. The width we obtained following this procedure can be assumed as the subsurface rupture width of *Wells and Coppersmith* [1994]. Once this parameter was fixed, we were able to evaluate the moment magnitude and, hence, the length (subsurface rupture length) trough the empirical relationships of *Wells and Coppersmith* [1994]. The aspect ratio of the fault dimensions obtained in this way is within the natural variability as shown by world-wide earthquake datasets [e.g. *Nicol et al*., 1996].

Strike and dip direction of the two modeled faults were derived from geological maps, geological cross sections and geophysical data (reference faults). Both the best position and the number of potentially active fault segments for each fault were chosen starting from the reference fault and proceeding with a step of 1 km along their strike (Section 2 in Figure 6). Besides, we envisaged the possibility that the terraces were deformed by structures which do not coincide with the reference faults, such as blind or off-trace segments. For this reason, we looked for the position of the best-fit fault segments in a NE-SW direction orthogonal to the reference faults, moving in a 4 km large window with a 0.5 km step (Section 3 in Figure 6). At each new position of the fault segments, strike, dip and rake were slightly adjusted to account for the internal geometric variations of the fault.

Altogether, 558613 fault models were scrutinized with a dedicated Visual Basic application to find the model that minimizes the difference between marine terraces elevation and predicted vertical displacement. This difference was estimated through a mean square deviation approach. The mathematic basis of the iterative fault model is described in Appendix C. All the tested fault models were evaluated against the best morphological marker available in the area, that is the MIS 5.5 paleo-shoreline (T4), whose elevation was corrected site-by-site for the regional uplift component as described in section 4.2. In this way, only the local vertical displacement (elevation difference between paleo-shoreline and regional uplift curve) was modeled (Section 2 in Figure 4).

5.3. Comparison with observational data

Along the Pollino coastal range, the best model solution for the local coastal deformation is represented by the two fault segments STF1 and VF1 (Figure 7 and Table 4). The imposed ~NNE-SSW trending shortening axis outcomes in almost pure reverse motion along the fault segments (see theoretical focal mechanisms in Figure 7).

Slip on the fault segments results in active uplift of two fault-propagation folds beneath the coast (Pollino and Valsinni anticlines; Figure 7 and Section 1 in Figure 8a). The Pollino anticline is underlain by the southwest-displacing STF1. This fault is modeled as a blind thrust extending from 1 to 7 km depth with a dip of 40°, a length of 16.9 km, a slip rate of 0.5 mm/a, and a maximum expected moment magnitude of 6.3 (Table 4). Vertical uplift caused by the STF1 is restricted to a narrow sector centered at the boundary between the Pollino Range and the Sibari Plain, with only a very limited subsidence north and south of the anticline (Section 2 in Figure 8a).

On the other hand, the Valsinni anticline has grown above the northeastern-displacing VF1 (Figure 7), which has a length of 8.7 km, a plane extending from 3 to 8 km with a southward dip of 60°, a slip rate of 0.7 mm/a, and a maximum expected moment magnitude of 5.9 (Table 4). Like the STF1, slip on the VF1 is responsible for a narrow belt of uplift, albeit of a slightly lesser amplitude, centered in the northern Pollino Range at the border with the San Nicola Plain (Section 2 in Figure 8a). No significant subsidence is expected north of the anticline (Section 2 in Figure 8a).

The modeled slip on the thrust faults reproduces with fair accuracy not only the MIS 5.5 paleo-shoreline shape, through which the model itself was tested, but also the elevation trend of terraces from T2 to T8 (Figure 8b and Sections 1 and 2 in Figure 8c). Conversely, because of their more limited spatial extent and the larger elevation uncertainties due to alluvial cover and human settlements, it was not possible to apply the fault model to the two younger terraces preserved along the southern Pollino coast (Figure 3): T1 (MIS 3.5; ~60 ka) and T0 (MIS 1; ~6 ka). Nevertheless, the sudden increase in elevation of T1, and to a lesser extent of T0 moving southward across the STF1 (Sections 3 and 4 in Figures 8c, respectively) suggests fault activity also during the latest Pleistocene-Holocene.

In order to evaluate the fault-induced uplift of T1 and T0 across the STF1, we estimated a nominal elevation due to the regional displacement for these terraces at the San Nicola Plain using the regional uplift rate derived at this location from the MIS 5.5 terrace (~0.6 mm/a). Considering age and eustatic depth of T1 (60.5 ka; -36 m b.s.l.) and T0 (5.9 ka; -5.3 m b.s.l.), we obtained nominal elevations of ~1.4 m a.s.l. and ~-1.7 m b.s.l., respectively.

Because the uncertainties on elevation estimates can be significant on the younger terraces, we preferred to consider for T1 the minimum local vertical displacement (Section 3 in Figure 8c; T1: 15 m). As far as T0, because of the large uncertainty on the Holocene displacement, which can incorporate un-modeled glacial-hydro-isostatic compensation components, we did not derive quantitative rate estimate across the STF1. Notwithstanding, the position of T1 and T0 above the elevation predicted by the regional uplift curve (Sections 3 and 4 in Figures 8c) is a robust evidence of vertical displacement accrued by the STF1 during the Holocene. This contention agrees with previous studies in the Sibari Plain [*Ferranti et al*., 2011] and at Roseto Capo Spulico [*Ferranti and Antonioli*, 2009], where uplifted coastal markers suggest uplift rates higher than the regional signal during the Holocene (Figure 2a).

With regard to the southernmost anticline (labeled as 3 in Figures 2a and 3), highlighted by the paleo-shoreline trends along the western border of the Sibari Plain, no transpressive system is known which can explain this local deformation. The only structure having the potential to form the anticline is the Pollino-Castrovillari normal fault through footwall uplift. We tested this hypothesis by means of a vertical elastic displacement model bench-marked against the MIS 5.5 terrace (Sections 1 and 2 in Figure 8a). Our model for the Pollino-Castrovillari Fault, whose parameters are summarized in Table 5, predicts a zone of uplift in the sector where we found one of the major positive undulations in the paleo-shorelines profile (Figure 7 and Section 1 in Figure 8a). In Section 1 of Figure 8a it is possible to appreciate the good correlation between the model displacement curve and the increase in elevation of the MIS 5.5 paleo-shoreline moving southward from the Pollino range toward the Sibari Plain. Our model supports the results of *Cucci and Cinti* [1998] and *Cucci* [2004], which proposed the repeated reactivation of the Pollino-Castrovillari fault during the Late Pleistocene.

6. Discussion

6.1. Quantitative contribution of regional and local sources to deformation

Reconstruction and modeling of the deformation experienced by Middle Pleistocene to Holocene paleo-shorelines along the Ionian margin of the Southern Apennines provided quantitative estimates of the regional and fault-induced components contributing to the total uplift. The two components specifically interlace along the Pollino Range coast, where the current paleo-shorelines shape can be interpreted as due to the superposition, on the regional northeastward tilt, of fault propagation-folds. Our results confirm the contention of *Caputo and Bianca* [2005], *Ferranti et al*. [2009] and *Caputo et al*. [2010] that shortening in the Southern Apennines went on during the Middle-Late Pleistocene and, possibly, is still ongoing.

The regional and local uplift signals reported in Figure 9 for coastal stretches straddling individual fault segments are mean values for the last ~400 ka and are based on our reconstruction of the regional uplift trend for terraces from T2 (MIS 5.1; ~80 ka) to T8 (MIS 11; ~401 ka). As pointed out previously [*Cucci and Cinti*, 1998; *Ferranti et al*., 2009; *Santoro et al*., 2009], the uplift process is mainly controlled by a regional source: the local fault uplift rate reaches a maximum of only 27% of the total budget along the VF1 (Figure 9). Fault-induced uplift occurred at broadly comparable rates for the STF1 (0.24 mm/a) and the VF1 (0.28 mm/a).

We are aware that the position of the modeled fault segments and the estimation of their contribution to the uplift rate is in large part determined by the spatial distribution of marine terraces used to evaluate the model accuracy, and subordinately by the imposed kinematic parameters. On the other hand, landward and seaward of the coast, the lack of appropriate geomorphologic and geologic markers does not allow to constrain activity of the modeled faults. Nonetheless, the vertical displacement rate derived for each fault from the morphotectonic analysis is consistent with results from the seismic profile interpretation across the offshore extension of the STF1 and VF1 (Figure 5). Restoration of the vertical displacement experienced by Middle Pleistocene reflectors documents 0.26 and 0.30 mm/a along the AMF and SPBF, respectively [*Mazzella*, 2011], in close agreement with the rates stipulated along their coastal counterparts (Figure 9).

Finally, for the Pollino-Castrovillari fault, the total displacement accrued by marine terraces in the Sibari Plain is partitioned between an 88% of regional uplift and a remaining 12% of footwall elastic displacement.

6.2. Temporal changes and spatial migration of fault-induced deformation

The availability of multiple paleo-geodetic markers represented by stepped terraces dated back to the last ~400 ka offers a means to evaluate the change in displacement distribution on the modeled fault segments during progressive time intervals. We found that fault displacement rate not only changed through time for individual faults (and for the cumulative fault array), but also varied in a coordinate manner among them. Figures 10a and 10b show the time-partitioned vertical displacement rate related to the STF1 and VF1 in the time lag spanning the formation of two successive marine terraces.

For each time period the vertical displacement rate (V_{DR}) for individual faults was obtained from the following equation:

$$V_{DR} = \frac{\left[\left(N_{ev}^{Tx} - N_{ev}^{Ty}\right)C_{vd}\right]}{T}, \qquad (1)$$

where: N_{ev}^{Tx} and N_{ev}^{Ty} are the number of seismic events predicted by fault modeling to explain paleo-shorelines deformations of terraces T_x and T_y respectively; C_{vd} is the co-seismic vertical displacement (mm); T is the time elapsed (yr) between the formation of terraces T_x and T_y. V_{DR} values are reported in Figure 10.

The fault-related vertical uplift rate was not constant during time but occurred as an alternation of periods with more rapid (up to ~1.9 mm/a) and slower or null displacement (Figure 10). From ~330 to 200 ka, the STF1 accrued the largest deformation, but it was characterized by a sharp decrease in displacement rate since then. Conversely, the VF1, which was markedly active before ~330 ka, was almost quiescent between ~330 to 200 ka, and resumed activity afterwards.

Thus, periods of sustained deformation on one fault strand were coincident with quiescence on the other (Figures 10a and 10b). This observation is consistent with well-known models of stress shadowing between sub-parallel faults at a temporal scale (~100 ka) larger than typical seismic cycles of crustal structures [*Dolan et al*., 2007].

During the last 80 ka, the STF1 and VF1 are characterized by comparable, limited displacement rates (0.26 and 0.20 mm/a, respectively). This results is replicated for the STF1 by an estimated 0.20 mm/a vertical displacement rate during the last 60 ka (Section 3 in Figure 8c). Although the accurate physical significance of this observation is not completely understood, and caution must be exercised because of the lack of precise age and position constraints for the younger terraces, we speculate that the coastal fault systems along the Pollino coast may be witnessing as a whole a period of healing. Building on this, we further suggest that crustal deformation is being transferred to laterally adjacent fault strands, possibly in the offshore sector, where earthquakes appear concentrated [*Ferranti et al.,* 2009].

6.3. Seismotectonic implications

The documentation of Late Pleistocene shortening on the eastern side of northern Calabria brings important implications for the seismotectonic and seismic hazard evaluation of the region, which is characterized by a low level of historical and instrumental seismicity. However, a few Mw 5-6 historical events localized in the coastal area north of the Sila Massif and in its offshore (CPTI, 2011) testify of the presence of seismogenic structures able to generate moderate but damaging earthquakes. The damage distribution and the effects associated with some of these events show that they may have been sourced by the fault system that includes the modeled coastal segments, and stretches to the east in the offshore area [*Ferranti et al.,* 2009]. Although we stress the difficulty of locating offshore historical and instrumental earthquakes, due to the uncompleted macroseismic field and the poor seismological constraints [e.g. *Fracassi et al*., 2012], this contention is consistent with the hypothesized recent shift of significant activity from the coastal to the offshore portion of the fault system.

A major uncertainty related to this issue regards the seismic behavior of the studied structures. When we consider the expected 5.9 to 6.3 moment magnitude (Mw) of the modeled fault segments (Table 4) derived from scalar relationships [e.g. *Wells and Coppersmith*, 1994], and the significant extent of the combined coastal and offshore fault system (Figure 2a), the contrast with the lack of historical and instrumental seismic moment released in the region is apparent (Figure 1). Obviously, this discrepancy might be mitigated by the observation that fault modeling of geologic or geomorphic markers based on elastic deformation [*Okada*, 1985], often results in an overestimation of Mw, since it does not consider the possibility that energy is released through micro-seismic or aseismic processes.

Moreover, historical reconstruction of settlement distribution in the Apennines indicates that the beginning of the 14th century marks a general cultural and economical development [*Cinti et al.*, 2002]; therefore, the occurrence of an earthquake in the magnitude range estimated for the fault system since 1300 AD would probably have been reported in the historical record, even in sparsely settled regions. In northern Calabria, several small settlements already existed prior to 1300 AD [*Cinti et al.*, 2002], and because of the region's relatively favorable climatic and topographic conditions, it is likely that cultural centers able to report large earthquakes in the area were settled at least since 1200 AD.

Thus, by combining historical, geomorphic and modeling data we suggest that major (Mw 5.9-6.3) seismic events along the PCF, STF1 and VF1 since 1200 A.D. may be unknown because: 1) the recurrence time exceeds the completeness of historic catalog for the related magnitude; 2) an unknown percentage of the accrued deformation is gradually released through a-seismic and/or micro-seismic processes, thus decreasing the expected maximum co-seismic magnitude.

7. Conclusions

An integrated study based on morphometric analysis and fault numeric modeling was carried to shed light on the Middle Pleistocene-Holocene deformation affecting the southernmost area of the Apennines frontal sector. In a region characterized by a scarce geomorphic expression of active faulting and a low level of instrumental seismicity, the morphometric approach proved to be useful in order to unravel the more recent tectonic history. A site-by-site sedimentological analysis of the Middle Pleistocene terraced deposit permitted to extract, from the paleo-morphology linked to the previous tectonic phases, the subtle deformation signal related to the more recent tectonic evolution. This signal has been split in a regional (deep-crustal or slab-related) and a local (fault-induced) component.

The regional uplift process, determining an overall northeastward tilt of the coastal area (tilt rate: $3*10^{-3}$ m km^{-1} ka^{-1}), accounts for ~80% of the total uplift. The local signal, conversely, is represented by anticline folds with a maximum ~20 km wavelength and a ~200 m amplitude. Taking advantage of existing geological and geophysical data, this local component can be modeled through an elastic fault numeric approach. Fault model results indicate two anticlines controlled by buried thrusts (spatially coinciding with the Satanasso and Valsinni transpressional faults mapped at the surface), that accrued deformation under a NNE-SSW trending shortening axis. Our multidisciplinary investigation points to activity of the thrust segments up to the Late Pleistocene-Holocene times. In the time period investigated, local, fault-induced, vertical deformation was not constant but occurred as an alternation of more rapid (up to ~1.9 mm/a) and slower or null periods of vertical displacement rates. Remarkably, we found that not only the fault segments activity was not constant at the 400-ka scale, but also that deformation shifted during time between the two modeled fault segments.

Based on our results and on available geophysical data, it is reasonable to hypothesize that the modeled coastal fault segments together with other segments in the laterally adjacent offshore belt could be seismogenic, thus posing a serious threat to the adjacent coastal sectors. The lack of significant historical and instrumental seismicity in the region can be explained by the release of an unknown percentage of accrued strain by means of aseismic or micro-seismic slip. Thus, acknowledging that the elastic fault model can overestimate the maximum expected magnitudes, we propose that the modeled fault zones can be responsible of moderate-high intensity earthquakes, probably not registered in the historical record due to recurrence time interval exceeding the record length.

Appendix A: Geochronological issues on the age of uplifted terraces

In Appendix A we fully explain the reasons for preferring the *Hearty et al*. [1986] aminozone scheme and for discarding some published dates along the coast of the Taranto Gulf.

Aminozone schemes

In the northern Taranto Gulf *Hearty et al*. [1986] established local aminozones based on 3 U-series dating of *Cladocora caespitosa* sampled at Il Fronte, Mare Piccolo. Corals incorporate uranium into their aragonite exoskeletons in equilibrium with the uranium oceanic content during the life cycle, and then behave as radiometric closed systems until aragonite is transformed into calcite. For this reason, unrecrystallized fossil corals (calcite content <3%) are, generally, considered the best material for U/Th dating. The above mentioned U/Th ages were first presented by *Hearty and Dai Pra* [1985]; in situ coral samples were collected in a level rich in *Persististrombus latus* [*Gmelin*, 1971]. The three *Cladocora caespitosa* U/Th ages (117±7 ka, 128±7 ka and 121±7 ka) result in a mean value of 122±4 ka and are all concordant with the attribution of Il Fronte section to the MIS 5.5 (~124 ka). These age determinations substantially refined previous corals U/Th ages presented by *Dai Pra and Stearns* [1977] for the same section (87±4 ka, 106±8 ka, 130±10 ka and 154±13 ka). It is not easy to determine whether the major scatter of these older dates represent several marine episodes centered around the Last Interglacial or analytical variability dependent on the major uncertainty about U-series method at the time, when potential problems of this technique applied to coral samples were not yet fully realized. Notwithstanding, we believe that the attribution of the Il Fronte section to the Last Interglacial, based on the available U-series ages, is strongly constrained. Regarding to the aminozones, *Hearty et al*. [1986] correlated the Last Interglacial deposits in the Taranto Gulf to their aminozone E and, specifically, to a *Glycymeris* alle/ille ratio of 0.38±0.02. Overall, the extent of leucine epimerization for the aminozone E was based on 41 *Glycymeris* and 28 *Arca* specimens. Four additional aminozones were established in this area: C, 0.30±0.02 (MIS 5.1/5.3); F, 0.50±0.02 (MIS 7); G, 0.58±0.02 (MIS 9) and K, 1.09±0.09 (Early Pleistocene). Besides, *Hearty et al*. [1986], based on 7 *Cladocora caespitosa* U/Th ages and 389 amino acid racemization analysis, extended the aminozone definition to the entire Mediterranean area.

The *Hearty et al.* [1986] aminozone scheme for the Taranto Gulf fits with amino acid data coming from Mediterranean sites were an independent chronology is well established. Because the extent of racemization is a temperature-dependent process, we focus our discussion on MIS 5.5 stratigraphic sections characterized by a similar mean annual temperature (MAT). For example, when we compare the Taranto Gulf with the San Grauet section of the Mallorca island (MATs: 16.9° and 16.8°, respectively), we found the same extent of leucine epimerization (alle/ille ratios for aminozone E of 0.38 and 0.37, respectively) in *Glycymeris* specimens. We remark that the correlation of the San Grauet section with the MIS 5.5 has been well established with U-series dating applied to 1 sample of *Cladocora caespitosa* (129±7 ka) [*Hearty et al*., 1986] and 3 samples of *Glycymeris violacescens* (112±7 ka, 102±7 ka and 135+14/-10 ka) [*Hoang and Hearty,* 1989]. Besides, a reasonable agreement also exists with data from Cagliari in southern Sardinia. Here, a stratigraphic section hosting *Persististrombus latus* is independently attributed to the Last Interglacial based on *Cladocora caespitosa* U/Th ages (138±8 ka) [*Ulzega and Hearty*, 1986] and Electro spin Resonance (ESR) applied on *Arca Noae*, *Arca Tetragona* and *Glycymeris* (mean age: 112 ka) [*Orrù et al*., 2011]. In the same section a larger leucine epimerization ratio (alle/ille: 0.42) with respect to the Taranto Gulf is in agreement with the slightly higher MAT (17.5°).

Finally, the aminozone scheme of *Hearty et al*. [1986] for the Taranto Gulf is further supported by its accordance with global isoleucine epimerization data relative to the Last Interglacial [*Murray-Wallace*, 1995].

Belluomini et al. [2002] proposed a new aminozone scheme for the Taranto Gulf based on 65 alle/ille ratios determinations on *Glycymeris*, *Arca* and *Cerastoderma* specimens, calibrated with U/Th ages of 3 samples of *Cladocora caespitosa* and 4 mollusk shells (*Glycymeris* and *Pinna*). They established the following correlation between alle/ille ratios and eustatic highstands: MIS 3 (0.20-0.31), 5.1 (0.34-0.38), 5.3 (0.41-0.44) and 5.5 (0.48-0.55).

We believe, however, that severe pitfalls are embedded within the *Belluomini et al*. [2002] aminozones definition. The scheme could be influenced by an age underestimation caused by a continuous or recent uranium uptake by the analyzed mollusks acting as radioactive open systems during diagenetic processes. Unlike corals, mollusk shells contain little authigenic U and their bulk U content essentially represent early diagenetic uptake [*Kaufman et al*., 1996]. It has been suggested that this uptake occurs within a few thousand years [*Broecker*, 1963] and perhaps up to 10 ka after death [*Ivanovich et al*., 1983]. If after this early U uptake mollusks act as closed systems for the duration of their diagenetic history, they can be used for chronological purposes [*Szabo and Rosholt*, 1969]. In his seminal work, *Kaufman et al*. [1971], by reviewing U-series ages of 400 mollusks, concluded, on the basis of internal inconsistencies with absolute and stratigraphic ages, that ^{230}Th/U ages of mollusks are generally unreliable. Similarly, *McLaren and Rowe* [1996] demonstrated the unreliability of mollusks U-series ages in the Mediterranean area. On the other hand, consistent and reproducible results were obtained by *Kaufman et al*. [1996] and *Hillaire-Mercel et al*. [1996]. It was shown that U-uptake mechanisms may differ between taxa [*Hillarie-Mercel et al*., 1996; *McLaren and Rowe*, 1996] and species of the same taxa [*Hoang and Hearty*, 1989], possibly in relation to the porosity of the shell and/or to the specific rate of organic lining decay. Therefore, it is necessary to check the validity of mollusks U-series dating through the analysis of different samples of various taxa collected from the same stratigraphic level as well as by comparing results with ages derived from different dating methods.

These kind of tests are absent in *Belluomini et al*. [2002] who analyzed only 4 samples (*Glycymeris* and *Arca*), collected from three different stratigraphic levels and with ages substantially lower than the *Cladocora caespitosa* U/Th ages obtained by *Hearty and Dai Pra* [1985] at Il Fronte section. Furthermore, *Hoang and Hearty* [1989] had already demonstrated the unreliability of U/Th ages applied on *Glycymeris* in a stratigraphic section located inside the area studied later by *Belluomini et al*. [2002].

Finally, if we accept the aminozone scheme and the U/Th ages of *Belluomini et al.* [2002], a straightforward problem arise by their disagreement both with Mediterranean sites where chronology is firmly established (see for instance the sites of Cagliari and Mallorca discussed above) and global isoleucine data [*Murray-Wallace*, 1995].

Discarded ages

In the study area, five sites where ages are available were not considered in our chronological scheme (sites AM97-1, CA10 and ZA06-1-2-3). Between the Basento and Cavone rivers, just north of the study area, our terraces T2, T3 and T4 were sampled by *Zander et al*. [2006] for Optically Stimulated Luminescence (OSL) dating techniques (sites ZA06-1, ZA06-2 and ZA06-3, respectively, in Figure 2b). The application of single aliquot regeneration (SAR) protocols and multiple aliquot additive (MAA) protocols on coarse grain potassium feldspars and SAR protocols on quartz did not bring significant information about terrace chronology. Regarding to the MAA quartz results, the authors stated that they are not reliable because the strong exponential shape of the saturating growth curves indicates a close to saturation level. With regard to the OSL dating results on potassium feldspars, in spite of the general agreement between SAR and MAA protocols, they fail in distinguishing by a chronological point of view terraces T2 and T3 (La Petrulla and San Teodoro I terraces in *Zander et al*. [2006]). Although a small age increase is detectable in the OSL feldspar results for our terrace T4 (San Teodoro II terrace in *Zander et al*. [2006]) with respect to

T2 and T3, SAR and MAA ages do not show a stratigraphic order in the coastal depositional sequence. Because of the evident age underestimation, probably caused by unstable luminescence centers in the feldspars and fading effects, the authors admitted the impossibility to establish a reliable chrono-stratigraphic frame for the terrace flight. According to their conclusions, we did not consider their ages in our chronological scheme.

Between the Agri and Cavone rivers, *Caputo et al*. [2010] obtained an AMS ^{14}C age of >42 ka from a *Pecten* sp. collected at the outer margin of our terrace T2 (site CA10 in Figure 2b). Radiocarbon dating of material aged >25–30 ka BP can be problematic because of several principal influences. Perhaps the most significant is contamination of carbonaceous material by exogenous carbon, the extent to which it has become chemically associated or cross-linked and the success of radiocarbon pre-treatment chemistry in removing it. Furthermore, the calibration of ^{14}C age >25–30 ka BP is problematic because of the uncertainty about the ^{14}C concentration in the Earth's atmosphere in this period. For example, *Giaccio et al*. [2006] and *Pyle et al*. [2006] brought evidences of larger changes in atmospheric ^{14}C historic levels than previously attested, probably related to geomagnetic excursions. For these reasons and as suggested by *Caputo et al*. [2010] themselves, their AMS ^{14}C age poses only a minimum age limit to the relative coastal depositional sequence and does not bring substantial information about terrace chronology.

On the northern slope of the Pollino range, *Amato et al*. [1997] estimated the alle/ille ratios on 4 samples of *Glycymeris* sp. collected from the outer margin of our terrace T5 (110 m a.s.l.), about 4 km NW of Roseto Capo Spulico village (site AM97-1 in Figure 2a). The alle/ille ratio of 0.29±0.02 for the site AM97-1 corresponds, according to the *Hearty et al*. [1986] aminozone scheme, to MIS 5.1/5.3. Based on geomorphological considerations, the authors recognized a substantial underestimation in this age estimate. Hence, this site was not considered in our chronological scheme.

Appendix B: Depth conversion of seismic profile F75-89

The TWT F75-89 profile was depth converted based on a standard multi-phase velocity analysis. In order to define the actual thickness of single layers and assign them a velocity value, starting from the velocity readings at individual shot points where available, we computed every 200 ms the interval velocity at each point, by the Dix formula [*Dix*, 1955] simplified for horizontal strata:

$$v_{\text{int}} = \sqrt{\frac{\left[(v_2)^2 t_2\right] - \left[(v_1)^2 t_1\right]}{t_2 - t_1}}, \qquad \text{(B1)}$$

where: v_{int} is the interval velocity for each layer; v_1 and v_2 are stacking velocity values for the upper and lower layer boundaries; t_1 and t_2 are two-way travel time values down to the upper and lower boundaries. With these values we generated an isovelocity contour map using a Surfer-based triangulation with linear interpolation. We geometrically overlaid this map to the seismic profile in order to manually improve the automatic contour, eliminating computational errors through picking and smoothing of the curvatures. Finally, the manual contour map was re-interpolated to produce a final contour of isovelocities. On this base, the contour was manually converted into fields of color, each of them identifying a velocity body; this image was imported in a dedicated software (depthcon2000) that recognizes the chromatic scale associated to a specific velocity and converts the time image (both the interpolated and original seismic profile) into a depth calibrated image.

Identification in the depth profile of prominent horizons was calibrated with nearby oil-exploration well logs (Francesca, Franca and Lucia wells, Section 1 in Figure 2a). Occasional bio-stratigraphic and lithologic observations offer excellent markers that can be laterally traced along the profile and allow to assess the deformation rates across faults and folds.

Appendix C: Iterative fault model

The iterative fault model is based on the following mathematic theory. Considering a paleo-shoreline of *np* points and a certain number (*nL*) of vertical deformation models (hereafter Layers;

L), we want to determine the coefficients (number of seismic events) of the Layers linear combination that best approximate the marine terraces elevation. The solution of the problem is represented by the absolute minimum of the following equation:

$$F(\alpha_1,\alpha_2,..\alpha_{nl}) = \sum_{p=1}^{np}\left(\sum_{l=1}^{nl}\alpha_1 L_{l,p} - R_p\right)^2 , \tag{C1}$$

where, (x_i, y_i) are the points of a shoreline, R_i is the elevation of the shoreline in the i^{th} point, L_{ij} is the elevation of the layer (vertical deformation model) j^{th} in the i^{th} point and $(\alpha_1,\alpha_2,...\alpha_{nl})$ are the linear combination coefficients that we want to determine. Given that equation 2 is the function of an hyperbolic paraboloid, it is characterized by only a minimum, that is the absolute minimum that guarantees the solution of the problem. The approximations between vertical displacement models and terraces elevation were estimated using the following equation:

$$G(\alpha_1,\alpha_2,..\alpha_{nl}) = \sum_{p=1}^{np}\left(\sum_{l=1}^{nl}\alpha_1 L_{l,p} - R_p\right). \tag{C2}$$

In order to determine the absolute minimum of equation 2 we used the followed procedure:

1. for each *l* = 1.....*nl*, we calculated the partial derivative of function *F*:

$$\frac{\delta F}{\delta \alpha_l}\sum_{p=1}^{np}\left[L_{k,p}2\left(\sum_{l=1}^{nl}\alpha_l L_{l,p} - R_p\right)\right] = 2\sum_{p=1}^{np}\left(\sum_{l=1}^{nl}\alpha_l L_{k,p}L_{l,p} - L_{k,p}R_p\right) = 2\left(\sum_{p=1}^{np}\sum_{l=1}^{nl}\alpha_l L_{k,p}L_{l,p} - \sum_{p=1}^{np}L_{k,p}R_p\right); \tag{C3}$$

2. we obtained a system of *nl* equations in *nl* unknowns. The absolute minimum was found solving the following system:

$$\begin{cases} \sum_{p=1}^{np}\sum_{l=1}^{nl}\alpha_l L_{1,p}L_{l,p} - \sum_{p=1}^{np}L_{1,p}R_p = 0 \\ \sum_{p=1}^{np}\sum_{l=1}^{nl}\alpha_l L_{2,p}L_{l,p} - \sum_{p=1}^{np}L_{2,p}R_p = 0 \\ \cdots\cdots\cdots\cdots\cdots\cdots\cdots\cdots \\ \sum_{p=1}^{np}\sum_{l=1}^{nl}\alpha_l L_{nl,p}L_{l,p} - \sum_{p=1}^{np}L_{nl,p}R_p = 0 \end{cases} . \tag{C4}$$

References

Amato, A., G. Belluomini, A. Cinque, M. Manolio, and F. Ravera (1997), Terrazzi marini e sollevamenti tettonici quaternari lungo il margine ionico dell’Appennino Lucano, *Il Quaternario, 10 (2)*, 329 – 336.

Antonioli, F., L. Ferranti, A. Fontana, A. Amorosi, A. Bondesan, C. Braitenberg, A. Dutton, G. Fontolan, S. Furlani, K. Lambeck, G. Mastronuzzi, C. Monaco, G. Spada, and P. Stocchi (2009), Holocene relative sea-level changes and vertical movements along the Italian and Istrian coastlines, *Quaternary International*, *206 (1-2)*, 102 – 133, doi:10.1016/j.quaint.2008.11.008.

Belluomini, G., M. Caldara, C. Casini, M. Cerasoli, L. Manfra, G. Mastronuzzi, G. Palmentola, P. Sanso, P. Tuccimei, and P. L. Vesica (2002), The age of Late Pleistocene shorelines and tectonic activity of Taranto area, Southern Italy, *Quaternary Science Reviews*, *21*, 525 – 547.

Benedetti, L., P. Tapponier, G. C. P. King, B. Meyer, and I. Manighetti (2000), Growth folding and active thrusting in the Montello region, Veneto, northern Italy, *J. Geophys. Res.*, *105(B1)*, 739 – 766, doi:10.1029/1999JB900222.

Bentivenga, M., M. Coltorti, G. Prosser, and E. Tavarnelli (2004), A new interpretation of terraces in the Taranto Gulf: the role of extensional faulting, *Geomorphology*, *60*, 383 – 402, doi:10.1016/j.geomorph.2003.10.002.

Bianca, M., and R. Caputo (2003), Analisi morfotettonica ed evoluzione quaternaria della Val d'Agri, Appennino meridionale, *Il Quaternario*, *16 (2)*, 158 – 170.

Bigi, G., G. Bonardini, R. Catalano, D. Cosentino, F. Lentini, M. Parlotto, R. Sartori, P. Scandone, and E. Turco (1992), Structural Model of Italy, 1:500.000, *Consiglio Nazionale delle Ricerche*, Rome.

Boenzi, F., M. Caldara, and L. Pennetta (1985), La Trasgressione Tirreniana nei dintorni di Castellaneta (Taranto), *Geologia Applicata e Idrogeologia*, *20*, 163 – 175.

Broecker, W. S. (1963), A preliminary evaluation of uranium series inequilibrium as a tool for absolute age measurement on marine carbonates, *J. Geophys. Res.*, *68*, 2817 – 2834.

Brückner, H. (1980), Marine Terrassen in Süditalien. Eine quartärmorphologische Studie über das Küstentiefland von Metapont, *Dusseld. Geogr. Schr.*, *14*, 1 – 235.

Caldara, M. (1988), La sezione tirreniana di Ponte del Re (Castellaneta Marina, Taranto): analisi paleocologica, *Atti della Società Toscana Scienze Naturali Mem.*, *A 93*, 129 – 163.

Caputo, R., and M. Bianca (2005), Morphological evidence of Late Quaternary thrusting in the Bradanic Foredeep, *Rend. Soc. Geol. It.*, *1*, 75 – 76.

Caputo, R., M. Bianca, and R. D'Onofrio (2010), Ionian marine terraces of Southern Italy: insights into the Quaternary tectonic evolution of the area. *Tectonics*, *29*, TC4005, doi:10.1029/2009TC002625.

Catalano, R., C. Doglioni, and S. Merlini (2001), On the Mesozoic Ionian Basin, *Geophys. J. Int.*, *144*, 49 – 64, doi:10.1046/j.0956-540X.2000.01287.x.

Catalano, S., C. Monaco, L. Tortorici, and C. Tansi (1993), Pleistocene strike-slip tectonics in the Lucanian Apennine (Southern Italy), *Tectonics*, *12 (3)*, 656 – 665, doi:10.1029/92TC02251.

Cello, G., L. Tortorici, N. Martini, and W. Paltrinieri (1989), Structural style in the frontal zones of the southern Apennines, Italy: An example from the Molise district, *Tectonics*, *8*, 753 – 768.

Chiarabba, C., L. Jovane, and R. Di Stefano (2005), A new view of Italian seismicity using 20 years of instrumental recordings, *Tectonophysics*, *395 (3-4)*, 251 – 268, doi:10.1016/j.tecto.2004.09.013.

Chiarabba, C., P. De Gori, and F. Speranza (2008), The southern Tyrrhenian subduction zone: Deep geometry, magmatism, and Plio-Pleistocene evolution, *Earth Planet. Sci. Lett.*, *268*, 408 – 423, doi:10.1016/j.epsl.2008.01.036.

Cinti, F. R., L. Cucci, D. Pantosti, and G. D'Addezio (1995), What is the role played by the two seismogenic faults located in the seismic gap of the Pollino region (southern Italy)?, 1995 Fall Meeting, suppl. To EOS, Trans. Am. Geophys. Un., 76, F359.

Cinti, F. R., L. Cucci, D. Pantosti, G. D’Addezio, and M. Meghraoui (1997), A Major seismogenic fault in a ‘silent area’: the Castrovillari fault (southern Apennines, Italy), *Geophys. J. Int.*, *130*, 595 – 605, doi:10.1111/j.1365-246X.1997.tb01855.x.

Cinti, F. R., M. Moro, D. Pantosti, L. Cucci, and G. D’Addezio (2002), New constraints on the seismic history of the Castrovillari fault in the Pollino gap (Calabria, southern Italy), *Journal of Seismology*, *6*, 199 – 217, doi:10.1023/A:1015693127008.

Colella, A. (1988), Fault-controlled marine Gilbert-type fan deltas, *Geology, 16 (11),* 1031 – 1034, doi:10.1130/0091-7613(1988)016<1031:FCMGTF>2.3.CO;2.

Cotecchia, V., G. Dai Pra, and G. Magri (1969), Oscillazioni tirreniane ed oloceniche del livello mare nel Golfo di Taranto, corredate da datazioni con metodo del Radiocarbonio, *Geologia applicata e idrogeologia*, *4*, 93 – 148.

Cotecchia, V., G. Dai Pra, and G. Magri (1971), Sul Tirreniano della Costa ionica salentina (Puglia). Datazione di un campione di coralli col metodo Th/U, *Geologia Applicata e Idrogeologia*, *6*, 105 – 112.

Cucci, L. (2004), Raised marine terraces in the Northern Calabrian Arc (Southern Italy): a ~600 Kyr-long geological record of regional uplift, *Ann. Geophys.*, *47 (4)*, 1391 – 1406.

Cucci, L., and F. R. Cinti (1998), Regional uplift and local tectonic deformation recorded by the Quaternary marine terraces on the Ionian coast of northern Calabria (southern Italy). *Tectonophysics*, *292 (1-2)*, 67 – 83, doi:10.1016/S0040-1951(98)00061-4.

D'Agostino, N., and G. Selvaggi (2004), Crustal motion along the Eurasia–Nubia plate boundary In the Calabrian Arc and Sicily and active extension in the Messina Straits from GPS measurements, *J. Geophys. Res.*, *109*, B11402, doi:10.1029/2004JB002998.

D’Agostino, N., A. Avallone, D. Cheloni, E. D’Anastasio, S. Mantenuto, and G. Selvaggi (2008), Active tectonics of the Adriatic region from GPS and earthquake slip vectors, *Journal of Geophysical Research, 113*, B12413, doi:10.1029/2008JB005860.

Dai Pra, G. (1982), The Late Pleistocene marine deposits of Torre Castiglione (Puglia, Southern Italy), *Geografia Fisica Dinamica Quaternaria*, *5*, 115 – 119.

Dai Pra, G., and P. J. Hearty (1988), I livelli marini pleistocenici del Golfo di Taranto. Sintesi geocronostratigrafica e tettonica, *Memorie Società Geologica Italiana*, *41*, 637 – 644.

Dai Pra, G., and C. E. Stearns (1977), Sul Tirreniano di Taranto. Datazioni su coralli con il metodo del ^{230}Th/^{234}U, *Geologica Romana*, *16*, 231 – 242.

Del Ben, A., C. Barnaba, and A. Toboga (2007), Strike-slip systems as the main tectonic features in the Plio-Quaternary kinematics of the Calabrian Arc, *Mar. Geophys. Res.*, *29 (1)*, 1 – 12, doi:10.1007/s11001-007-9041-6.

Devoti, D., F. Riguzzi, M. Cuffaro, and C. Doglioni (2008), New GPS constraints on the kinematics of the Apennines subduction, *Earth Planet. Sci. Lett.*, *273 (1-2)*, 163 – 174, doi:10.1016/j.epsl.2008.06.031.

Dix, C. H. (1955), Seismic velocities from surface measurements, *Geophysics*, *20*, 68 – 86.

Dolan, J. F., D. D. Bowman, and C. G. Sammis (2007), Long-range and long-term fault interactions in Southern California, *Geology*, *35 (9)*, 855 – 858, doi:10.1130/G23789A.1.

Dubar, M., C. Innocent, and O. Sivan (2008), Radiometric dating (U/Th) of the lower marine terrace (MIS 5.5) west of Nice (French Riviera): Morphological and neotectonic quantitative implications, *C. R. Geoscience*, *340 (11)*, 723 – 731, doi:10.1016/j.crte.2008.07.012.

Ekström, G., R. S. Stein, J. P. Eaton, and D. Eberhart-Phillips (1992), Seismicity and geometry of a 110-km long blind thrust fault, 1. The 1985 Kettleman Hills, California, earthquake, *J. Geophys. Res.*, *97 (B4)*, 4843 – 4864, doi:10.1029/91JB02925.

Faccenna, C., T. W. Becker, F. P. Lucente, L. Jolivet, and F. Rossetti (2001), History of subduction and back-arc extension in the Central Mediterranean, *Geophys. J. Int.*, *145 (3)*, 809 – 820, doi:10.1046/j.0956-540x.2001.01435.x.

Faccenna, C., L. Civetta, M. D'Antonio, F. Funiciello, L. Margheriti, and C. Piromallo (2005), Constraints on mantle circulation around the deforming Calabrian slab, *Geophysical Research Letters*, *32*, L06311, doi:10.1029/2004GL021874.

Faccenna, C., P. Molin, B. Orecchio, V. Olivetti, O. Bellier, F. Funiciello, L. Minelli, C. Piromallo, and A. Billi (2011), Topography of the Calabria subduction zone (southern Italy): Clues for the origin of Mt. Etna, *Tectonics*, *30*, TC1003, doi:10.1029/2010TC002694.

Ferranti, L., and F. Antonioli (2009), First evidence for Holocene uplift in the Ionian Sea coast of northern Calabria: the notch at Roseto Capo Spulico, paper presented at FIST Geoitalia 2009, 7° Forum Italiano di Scienze della Terra, Rimini, 9-2009, *Epitome*, *3*, 153.

Ferranti, L., and J. S. Oldow (2005), Latest Miocene to Quaternary horizontal and vertical displacement rates during simultaneous contraction and extension in the Southern Apennines orogen, Italy, *Terra Nova*, *17*, 209 – 214.

Ferranti, L., F. Antonioli, B. Mauz, A. Amorosi, G. Dai Prà, G. Mastronuzzi, C. Monaco, P. Orrù, M. Pappalardo, U. Radtke, P. Renda, P. Romano, P. Sansò, and V. Verrubbi (2006), Markers of the last interglacial sea-level high stand along the coast of Italy: tectonic implications, *Quaternary International*, *145-146*, 30 – 54, doi:10.1016/j.quaint.2005.07.009.

Ferranti, L., C. Monaco, F. Antonioli, L. Maschio, S. Kershaw, and V. Verrubbi (2007), The Contribution of Regional Uplift and Coseismic Slip to the Vertical Crustal Motion in the Messina Straits, Southern Italy: Evidence from Raised Late Holocene Shorelines, *Journal of Geophysical Research*, *112*, B06401. doi:10.1029/2006JB004473.

Ferranti, L., J. S. Oldow, B. D'Argenio, R. Catalano, D. Lewis, E. Marsella, G. Avellone, L. Maschio, G. Pappone, F. Pepe, and A. Sulli (2008), Active deformation in Southern Italy, Sicily and southern Sardinia from GPS velocities of the Peri-Tyrrhenian Geodetic Array (PTGA), *Boll. Soc. Geol. It., (Ital. J. Geosci.)*, *127 (2)*, 299 – 316.

Ferranti, L., E. Santoro, M. E. Mazzella, C. Monaco, and D. Morelli (2009), Active transpression in the northern Calabria Apennines, southern Italy, *Tectonophysics*, *476 (1-2),* 226 – 251, doi:10.1016/j.tecto.2008.11.010.

Ferranti, L., F. Antonioli, M. Anzidei, C. Monaco, and P. Stocchi (2010), The timescale and spatial extent of vertical tectonic motions in Italy: insights from relative sea-level change studies. In: Beltrando, M., A. Peccerillo, M. Mattei, S. Conticelli, and C. Doglioni (Eds.), The Geology of Italy, *Journal of the Virtual Explorer*, ISSN: 1441 – 8142 36, Electronic Edition, *30*.

Ferranti, L., R. Pagliarulo, F. Antonioli, and A. Randisi (2011), "Punishment for the Sinner": Holocene episodic subsidence and steady tectonic motion at ancient Sybaris (Calabria, southern Italy), *Quaternary International*, *232 (1-2),* 56 – 70, doi:10.1016/j.quaint.2010.07.014.

Fracassi, U., D. Di Bucci, D. Ridente, F. Trincardi, and G. Valensise (2012), Recasting historical earthquakes in coastal areas (Gargano Promontory, Italy): Insights from marine paleoseismology, *Bull. Seismol. Soc. Am.*, 102 (1), doi: 10.1785/0120110001.

Frepoli, A., and A. Amato (2000), Fault plane solutions of crustal earthquakes in Southern Italy (1988–1995): seismotectonic implications, *Ann. Geophys.*, *43 (3)*, 437 – 468.

Frepoli, A., C. Maggi, G. B. Cimini, A. Marchetti, and M. Chiappini (2011), Seismotectonic of Southern Apennines from recent passive seismic experiments, *Journal of Geodynamics*, *51 (2-3)*, 110 – 124, doi:10.1016/j.jog.2010.02.007.

Gaki-Papanastassiou, K., E. Karymbalis, D. Papanastassiou, and H. Maroukian (2009), Quaternary marine terraces as indicators of neotectonic activity of the Ierapetra normal fault SE Crete (Greece), *Geomorphology*, *104 (1-2),* 38 – 46, doi:10.1016/j.geomorph.2008.05.037.

Galli, P., V. Spina, I. Ilardo, and G. Naso (2010), Evidence of active tectonics in Southern Italy: the Rossano fault (Calabria), in *Recent Progress on Earthquake Geology*, edited by Pierpaolo Guarnieri, pp. 49 – 78.

Giaccio, B., I. Hajdas, M. Peresani, F. G. Fedele, and R. Isaia (2006), The Campanian Ignimbrite tephra and its relevance for the timing of the Middle to Upper Palaeolithic shift. In:

Conard, N.J. (Ed.), When Neanderthals and Modern Humans Met. Kerns Verlag, Tübingen, 343 – 375.

Gignoux, M. (1913), Les formations marines pliocène et quaternaires de l'Italie du sud et de la Sicile, *Annals de l'Universitè de Lyon*, 36.

Gigout, M. (1960a), Sur le Quaternaire marin de Pulsano (Tarente, Italie), *Comptes rendus hebdomadaires de l'Acadèmie des sèances*, *250*, 881 – 883.

Gigout, M. (1960b), Sur le Quaternaire marin de Tarente (Italie), *Comptes rendus hebdomadaires de l'Acadèmie des sèances*, *250*, 1094 – 1096.

Gigout, M. (1960c), Sur le Quaternaire marin de Gallipoli (Italie), *Comptes rendus hebdomadaires de l'Acadèmie des sèances*, *250*, 1295 – 1297.

Gvirtzman, Z., and A. Nur (2001), Residual topography, lithospheric structure and sunken slabs in the central Mediterranean, *Earth Planet. Sci. Lett.*, *187 (1-2)*, 117 – 130, doi:10.1016/S0012-821X(01)00272-2.

Hauksson, E., and L. M. Jones (1989), The 1987 Whittier Narrows earthquake sequence in Los Angeles, southern California: seismological and tectonic analysis, *J. Geophys. Res.*, *94 (B7)*, 9569 – 9590, doi:10.1029/JB094iB07p09569.

Hearty, P. J. and G. Dai Pra (1985), Aminostratigraphy and Th/U dating of Quaternary shorelines in the Puglia region of Southeast Italy, paper presented at Fifth International Coral Reef Congress, Tahiti, *3*, 163 – 169.

Hearty, P. J., and G. Dai Pra (1992), The age and stratigraphy of middle Pleistocene and younger deposits along the Gulf of Taranto (southeast Italy), *Journal of Coastal Research*, *8 (4)*, 882 – 903.

Hearty, P. J., G. H. Miller, C. E. Stearns, and B. J. Szabo (1986), Aminostratigraphy of quaternary shorelines in the Mediterranean basins, *Geological Society of American Bullettin*, *97*, 850 – 858.

Hillaire-Marcel, C., C. Garièpy, B. Ghaleb, J. L. Goy, C. Zazo, and J. Cuerda Barcelo (1996), U-series measurements in Tyrrhenian deposits from Mallorca further evidence for two last-interglacial high sea levels in the Balearic Islands, *Quaternary Science Reviews*, *15*, 53 – 62.

Hippolyte, J. C., J. Angelier, and F. Roure (1994), A major geodynamic change revealed by Quaternary stress patterns in the Southern Apennines (Italy), *Tectonophysics*, *230 (3-4)*, 199 – 210, doi:10.1016/0040-1951(94)90135-X.

Hoang, C. T., and P. J. Hearty (1989), Uranium-series and amino acid dating comparisons from the ‘‘Il Fronte Formation’’ Puglia Italy, and Son Grauet, Mallorca, Spain, *Chemical Geology (Isotope Geoscience Section)*, *79*, 317 – 323.

Hollenstein, C., H. G. Kahle, A. Geiger, S. Jenny, S. Goes, and D. Giardini (2003), New GPS constraints on the Africa–Eurasia plate boundary in southern Italy, *Geophys. Res. Lett.*, *30 (18)*, 1935, doi:10.1029/2003GL017554.

Hunstad, I., G. Selvaggi, N. D'Agostino, P. England Clarke, and M. Pierozzi (2003), Geodetic strains in peninsular Italy between 1875 and 2001, *Geophys. Res. Lett.*, *30 (4)*, 1181, doi:10.1029/2002GL016447.

Ivanovich, M., C. Vita-Finzi, and G. J. Henning (1983), Uranium-series dating of molluscs from uplifted Holocene beaches in the Persian Gulf, *Nature*, *302*, 408 – 410.

Kaufman, A., W. S. Broecker, T. L. Ku, and D. L. Thurber (1971), The status of U-series methods of mollusk dating, *Geochimica et Cosmochimica Acta*, *35*, 1138 – 1155.

Kaufman, A., B. Ghaleb, J. F. Wehmiller, and C. Hillaire-Marcel (1996), Uranium concentration and isotope ratio profiles within Mercenaria shells: geochronological implications, *Geochimica et Cosmochimica Acta*, *60*, 3735 – 3746.

Keller, E. A., R. L. Zepeda, T. K. Rockwell, T. L. Ku, and W. S. Dinklage (1998), Active tectonics at Wheeler Ridge, southern San Joaquin, California, *Geol. Soc. Am. Bull.*, *110 (3)*, 298 – 310, doi:10.1130/0016-7606(1998)110<0298:ATAWRS>2.3.CO;2.

Kikuchi, M., H. Kanamori, and K. Satake (1993), Source Complexity on the 1988 Armenian Earthquake: Evidence for a Slow After-Slip Event, *Journal of Geophysical Research*, *98 (B9)*, 15,797 – 15,808.

Knott, S. D. (1987), The Liguride complex of Southern Italy-a Cretaceous to Paleogene accretionary wedge, *Tectonophysics*, *142 (2-4)*, 217 – 226, doi:10.1016/0040-1951(87)90124-7.

Knott, S. D., and E. Turco (1991), Late Cenozoic kinematics of the Calabrian arc, southern Italy, *Tectonics*, *10 (6)*, 1164 – 1172, doi:10.1029/91TC01535.

Lambeck, K., F. Antonioli, M. Anzidei, L. Ferranti, G. Leoni, and S. Silenzi (2011), Sea level change along the Italian coasts during Holocene and prediction for the future, *Quaternary International, 232 (1-2),* 250 – 257, doi:10.1016/j.quaint.2010.04.026.

Lisiecki, L. E. and M. E. Raymo (2005), A Pliocene-Pleistocene stack of 57 globally distributed benthic d^{18}O records, *Paleoceanography*, *20*, PA1003, doi:10.1029/2004PA001071.

Malinverno, A., and W. B. F. Ryan (1986), Extension in the Tyrrhenian Sea and shortening in the Apennines as a result of arc migration driven by sinking of the lithosphere, *Tectonics*, *5 (2)*, 227 – 245, doi:10.1029/TC005i002p00227.

Maschio, L., L. Ferranti, and P. Burrato (2005), Active extension in Val d'Agri area, Southern Apennines, Italy: implications for the geometry of the seismogenic belt, *Geophys. J. Int.*, *162 (2)*, 591 – 609, doi:10.1111/j.1365-246X.2005.02597.x.

Mastronuzzi, G. (2001), Indagine conoscitiva geologico-ambientale del sistema del mar Piccolo (Taranto), in Atelier Taranto, Comune di Taranto, Progetto 55 Posidonia, EU, DG 16, Azioni innovatrici.

Mastronuzzi, G., and P. Sansò (2003), Quaternary coastal morphology and sea level changes, Field Guide Puglia *2003*, Final Conference – Project IGCP 437 UNESCO – IUGS, Otranto/Taranto – Puglia (Italy) 22-28 September 2003, GI2S Coast – Gruppo Informale di Studi Costieri, *Research Publication*, *5*, pp. 184, Brizio srl – Taranto.

Mazzella, M. E. (2011), Tettonica attiva del settore peri tirrenico meridionale attraverso l'integrazione dei dati geodetici e geologici, PhD thesis, Dipartimento di Scienze della Terra, Università degli Studi di Napoli Federico II, Naples, Italy.

McLaren, S. J., and P. J. Rowe (1996), The reliability of Uranium-series mollusk dates from the Western Mediterranean basin, *Quaternary Science Reviews (Quaternaty Geochronology), 15*, 709 – 717.

Menardi-Noguera, A., and G. Rea (2000), Deep structure of the Campanian–Lucanian Arc (Southern Apennine, Italy), *Tectonophysics*, *324 (4)*, 239 – 265, doi:10.1016/S0040-1951(00)00137-2.

Michetti, A. M., L. Ferreli, L. Serva, and E. Vittori (1997), Geological evidence for strong historical earthquakes in an “aseismic” region: The Pollino case (Southern Italy), *Journal of Geodynamics*, *24*, 67 – 86.

Miyauchi, T., G. Dai Pra, and S. Sylos Labini (1994), Geochronology of Pleistocene marine terraces and regional tectonics in the Tyrrhenian coast of South Calabria, Italy, *II Quaternario*, *7*, 17 – 34.

Monaco, C. and L. Tortorici (2000), Active faulting in the Calabrian arc and eastern Sicily, *J. Geodyn.*, *29 (3-5)*, 407 – 424, doi:10.1016/S0264-3707(99)00052-6.

Monaco, C., L. Tortorici, and W. Paltrinieri (1998), Structural evolution of the Lucanian Apennines, southern Italy, *J. Struct. Geol.*, *20 (5)*, 617 – 638, doi:10.1016/S0191-8141(97)00105-3.

Murray-Wallace, C. V. (1995), Aminostratigraphy of Quaternary coastal sequences in Southern Australia – an overview, *Quaternary International*, *26*, 69 – 86.

Nicol, A., J. Watterson, J. J. Walsh, C. Childs (1996), The shapes, major axis orientations and displacement patterns of fault surfaces, *J. Struct. Geol.*, *18 (2-3)*, 235 – 248.

Okada, Y. (1985), Surface deformation due to shear and tensile faults in a half-space, *Bull. Seismol. Soc. Am.*, *75 (4)*, 1135 – 1154.

Oldow, J. S., L. Ferranti, D. Lewis, L. Campbell, B. D'Argenio, R. Catalano, G. Pappone, L. Carmignani, P. Conti, and C. Aiken (2002), Active fragmentation of Adria, the north African promontory, central Mediterranean orogen, *Geology, 30 (9)*, 779 – 782, doi:10.1130/0091-7613(2002)030<0779:AFOATN>2.0.CO;2.

Orrù, P. E., F. Antonioli, P. J. Hearty, and U. Radtke (2011), Chronostratigraphic confirmation of MIS 5 age of a baymouth bar at Is Arenas (Cagliari, Italy), *Quaternary International*, *232*, 169 – 178.

Papanikolaou, I. D. and G. P. Roberts (2007), Geometry, kinematics and deformation rates along the active normal fault system in the southern Apennines: implication for fault growth, *J. Struct. Geol.*, *29 (1)*, 166 – 188, doi:10.1016/j.jsg.2006.07.009.

Patacca, E., and P. Scandone (2001), Late thrust propagation and sedimentary response in the thrust belt-foredeep system of the Southern Apennines (Pliocene–Pleistocene), in *Anatomy of a Mountain Belt: the Apennines and Adjacent Mediterranean Basins*, edited by Vai, G. B., and I. P. Martini, Kluwer Academic Publishers, pp. 401 – 440.

Patacca, E., R. Sartori, and P. Scandone (1990), Tyrrhenian Basin and Apenninic arcs: kinematic relations since late Tortonian times, *Mem. Soc. Geol. Ital.*, *45*, 425 – 451.

Ponza, A., F. J. Pazzaglia, and V. Picotti (2010), Thrust-fold activity at the mountain front of the Northern Apennines (Italy) from quantitative landscape analysis, *Geomorphology*, *123 (3-4)*, 211 – 231, doi:10.1016/j.geomorph.2010.06.008.

Pyle, D. M., G. D. Ricketts, V. Margari, T. H. van Andel, A. A. Sinitsyn, N. D. Praslov, and S. Lisitsyn (2006), Wide dispersal and deposition of distal tephra during the Pleistocene 'Campanian Ignimbrite/Y5' eruption, Italy, *Quaternary Science Reviews*, *25 (21–22)*, 2713 – 2728.

Rockwell, T. K., E. A. Keller, and G. R. Dembroff (1988), Quaternary rate of folding of the Ventura Avenue anticline, western Transverse ranges, southern California, *Geol. Soc. Am. Bull.*, *100 (6)*, 850 – 858, doi:10.1130/0016-7606(1988)100<0850:QROFOT>2.3.CO;2

Saillard, M., S. R. Hall, L. Audin, D. L. Farber, V. Regard, and G. Hérail (2011), Andean coastal uplift and active tectonics in southern Peru: ^{10}Be surface exposure dating of differentially uplifted marine terrace sequences (San Juan de Marcona, ~15.4°S), *Geomorphology*, *128 (3-4)*, 178 – 190, doi:10.1016/j.geomorph.2011.01.004.

Santoro, E., M. E. Mazzella, L. Ferranti, A. Randisi, and E. Napolitano (2009), Raised coastal terraces along the Ionian Sea coast of northern Calabria, Italy, suggest space and time variability of tectonic uplift rates, *Quaternary International*, *206*, 78 – 101.

Selvaggi, G., and C. Chiarabba (1995), Seismicity and P-wave velocity image of the southern Tyrrhenian subduction zone, *Geophys. J. Int.*, *121 (3)*, 818 – 826, doi:10.1111/j.1365-246X.1995.tb06441.x

Stein, R. S., and G. C.P. King (1984), Seismic potential revealed by surface folding: 1983 Coalinga, California, earthquake, *Science*, *224 (4651)*, 869 – 872, doi:10.1126/science.224.4651.869.

Szabo, B. J., and J. N. Rosholt (1969), Uranium-series dating of Pleistocene molluscan shells from southern California – an open system model, *J. Geophys. Res.*, *76*, 3253 – 3260.

Tansi, C., F. Muto, S. Critelli, and G. Iovine (2007), Neogene–Quaternary strike-slip tectonics in the central Calabrian Arc (southern Italy), *J. Geodyn.*, *43 (3)*, 393 – 414, doi:10.1016/j.jog.2006.10.006.

Ulzega, A., and P. J. Hearty (1986), Geomorphology, Stratigraphy and Geochronology of Late Quaternary Marine Deposits in Sardinia, *Z. Geomorph. N. F., Suppl. Bd. 62*, 119 – 129.

Valensise, G., and S. N. Ward (1991), Long-term uplift of the Santa Cruz coastline in response to repeated earthquakes along the San Andreas Fault, *Bulletin of the Seismological Society of America*, *81 (5)*, 1694 – 1704.

Van Dijk, J. P., M. Bello, G. P. Brancaleoni, G. Cantarella, V. Costa, A. Frixa, F. Golfetto, S. Merlini, M. Riva, S. Torricelli, C. Toscano, and A. Zerilli (2000), A regional structural model for the northern sector of the Calabrian Arc (southern Italy), *Tectonophysics*, *324 (4)*, 267 – 320, doi:10.1016/S0040-1951(00)00139-6.

Verma, V. K. (1973), Map Parameters for correlation of marine terraces in California, *Geol. Soc. Am. Bull.*, *84 (8)*, 2737 – 2742, doi:10.1130/0016-7606(1973)84<2737:MPFCOM>2.0.CO;2.

Waelbroeck, C., L. Labeyrie, E. Michel, J. C. Duplessy, K. Lambeck, J. F. McManus, E. Balbon, and M. Labracherie (2002), Sea-level and deep water temperature changes derived from benthic foraminifera isotopic records, *Quaternary Science Reviews*, *21 (1-3)*, 295 – 305, doi:10.1016/S0277-3791(01)00101-9.

Ward, S. N. and G. Valensise (1996), Progressive growth of San Clemente Island, California, by blind thrust faulting: implications for fault slip partitioning in the California Continental Borderland, *Geophys. J. Int.*, *126 (3)*, 712 – 734, doi:10.1111/j.1365-246X.1996.tb04699.x.

Wehmiller, J. F., E. R. Thieler, D. Miller, V. Pellerito, V. Bakeman Keeney, S. R. Riggs, S. Culver, D. Mallinson, K. M. Farrell, L. L. Yor, J. Pierson, and P. R. Parham (2010), Aminostratigraphy of surface and subsurface Quaternary sediments, North Carolina coastal plain, USA, *Quaternary Geochronology*, *5 (4)*, 459 – 492.

Wells, D. L. and K. J. Coppersmith (1994), New empirical relationships among magnitude, rupture length, rupture width, rupture area, and surface displacement, *Bulletin of Seismological Society of America*, *84 (4)*, 974 – 1002.

Westaway, R. (1993), Quaternary uplift of southern Italy, *J. Geophys. Res.*, *98 (B12)*, 21741 – 21772, doi:10.1029/93JB01566.

Westaway, R., and D. Bridgland (2007), Late Cenozoic uplift of southern Italy deduced from fluvial and marine sediments: Coupling between surface processes and lower-crustal flow, *Quaternary International*, *175 (1)*, 86 – 124, doi:10.1016/j.quaint.2006.11.015.

Wortel, M. J. R., and W. Spakman (2000), Subduction and slab detachment in the Mediterranean–Carpathian region, *Science*, *290 (5498)*, 1910 – 1917, doi:10.1126/science.290.5498.1910.

Yielding, G., J. A. Jackson, G. C. P. King, H. Sinvhal, C. Vita-Finzi, and R. M. Wood (1981), Relations between surface deformation, fault geometry, seismicity, and rupture characteristics during the El Asnam (Algeria) earthquake of the 10 October 1980, *Earth and Planetary Science Letters*, *56*, 287 – 304, doi:10.1016/0012-821X(81)90135-7.

Yu, S. B., L. C. Kuo, Y. J. Hsu, H. H. Su, C. C. Liu, C. S. Huo, J. F. Lee, T. C., Lai, C. L., Liu, T. F. Tseng, C. S. Tsai, and T. C. Shin (2001), Preseismic deformation and coseismic displacements associated with the 1999 Chi-Chi, Taiwan earthquake, *Bull. Seismol. Soc. Am., 91 (5)*, 995 – 1012, doi:10.1785/0120000722.

Zander, A. M., A. Fülling, H. Brückner, and G. Mastronuzzi (2006), OSL dating of Upper Pleistocene littoral sediments: A contribution to the chronostratigraphy of raised marine terraces bordering the Gulf of Taranto, South Italy, *Geogr. Fis. Dinam. Quat.*, *29*, 33 – 50.

Figure 1. Tectonic map of the frontal Southern Apennines in the Calabria-Lucania sector. Active normal faults (barbs on downthrown side) after *Monaco and Tortorici* [2000], *Ferranti and Oldow* [2005], and the DISS database (http://legacy.ingv.it/DISS/). Strike-slip faults in the Pollino range after *Catalano et al*. [1993]. Rossano-Corigliano Fault (RCF), after *Galli et al*. [2010]. Other faults and geology after *Bigi et al*. [1992]. FE09-1-2-3, Early-Middle Pleistocene shortening axis, after *Ferranti et al*. [2009]. Dating sites: SA09, after *Santoro et al*. [2009]. Faults: CF, Civita Fault; CNNF, Canna Fault; PCF, Pollino-Castrovillari Fault; PF, Pagliara Fault; SRF, Saraceno Fault; STF, Satanasso Fault; VF, Valsinni Fault. DSSGD, deep-seated slope gravitational deformation. Villages: CC, Corigliano Calabro; SA, Spezzano Albanese; VA, Vaccarizzo Albanese. Section 1: Regional tectonic setting of southern Italy, showing the isobaths of the Ionian slab (redrawn after *Ferranti et al*. [2007]) and the margins of the Ionian basins (after *Catalano et al*. [2001]). Section 2:

Seismotectonic setting of the region. Focal solutions: CMT, Harvard CMT catalogue; FR-AM00, *Frepoli and Amato* [2000]; RCMT, European-Mediterranean RCMT catalogue.

Figure 2a. Morpho-structural map of the southern Apennines between the Sibari and San Nicola plains (location in Figure 1). Bathymetric and structural data for the offshore area modified after *Ferranti et al*. [2009]. The trace of section A-B against which the terraces paleo-shorelines are projected (Figure 3) and the trace of seismic reflection profile F75-89 (Figure 5) are reported. Major terraces positive undulations (labeled as in Figure 3) are localized along the Sibari Plain western border (3), the southern Pollino flank (2) and the Valsinni Ridge (1). Red stars indicate the position of uplifted Late Holocene coastal markers after *Ferranti et al*. [2011] (A) and *Ferranti and Antonioli* [2009] (B). Faults: AMF, Amendolara Fault; SBF: Sibari Basin Fault; SPBF: Spulico Basin Fault. Other faults labeled as in Figure 1. AMR: Amendolara Ridge. SB: Sibari Basin. Dating sites: AM97-1, *Amato et al*. [1997]; CU04, *Cucci* [2004]. Section 1: Grid of seismic profiles and wells location (http://unmig.sviluppoeconomico.gov.it/videpi/pozzi/consultabili.asp) used for constructing the offshore structural map [from *Ferranti et al*., 2009].

Figure 2b. Morphological map of Middle-Late Pleistocene marine terraces along the southern border of the San Nicola Plain (location in Figure 2a). The map trace and elevation of morphological inner margins are also reported. Note that morphological inner margins of terraces T2, T3 and T4 north of the Cavone river are inferred on topographic basis and are traced to compare our terraces to the dating sites available in this sector. Dating sites: AM97-2, *Amato et al*. [1997]; BR80, *Brückner*, [1980]; CA10, *Caputo et al*. [2010]; DP88, *Dai Pra and Hearty*, [1988]; ZA06-1-2-3, *Zander et al*. [2006].

Figure 3. Coast-parallel profiles of Middle Pleistocene-Holocene terraces inner edge elevation in northeastern Calabria and southeastern Basilicata. Distance, here and in other figures, is shown

from A to B along the trace of Figure 2a. Major paleo-shorelines undulations numbered as in Figure 2a. Section 1: Paleo-shorelines profiles of T0, T1 and T2 terraces along the Pollino Range (location in Figure 3).

Figure 4. Section1: Elevation-distance plot of the MIS 5.5 terrace along the Ionian coast (from north to south: northern Taranto Gulf, southern San Nicola Plain and northern Sila slope). Section 2: comparison between the MIS 5.5 terrace (T4) elevation and the derived regional uplift trend along the Pollino and San Nicola coastal stretches. The modeled local deformation (elevation difference between the terrace and the regional uplift curve) is evidenced in grey. Section 3: graphical representation of the regional gradient of terraces T2-T8 used for fault modeling. The horizontal distances and the elevation are exaggerated in order to better show the differences in regional gradient between terrace orders.

Figure 5. Southwestern portion of the depth-converted seismic reflection profile F75-89 (Section 1) and its line-drawing (Section 2). Faults labeled as in Figure 1. Position of oil-explorations wells projected along the section is also reported. Seismic line trace in Figure 2a.

Figure 6. Section 1: Fault segments modeled for each transpressive shear zone crossing the Pollino coastal area. Section 2: example of numeric models performed along the strike of the selected faults (STF and VF) in order to find number and geographic position of the best fit segments (see text for further details). Section 3: same as Section 2, performed across the strike. Centroids of the modeled faults are reported for the modeled segments in Sections 2 and 3. Faults labeled as in Figure 1.

Figure 7. Best fault segments and cumulative vertical fold-related displacement in the last 124 ka resulting from the iterative procedure described in the text. Theoretical focal solutions are also

reported with nodal planes, rake (arrows show the movement of the hanging wall) and positions of maximum (3), intermediate (2) and minimum (1) extensional axes.

Figure 8a. Section 1: Fault modeling results compared with the MIS 5.5 paleo-shoreline elevation trend. The vertical cumulative fold-related displacement curve is the sum of regional uplift and local fault-induced displacement. The position and depth extent (scale on the right of diagram) of the modeled faults and the regional uplift curve and rates (large arrows) are also reported. Section 2: spatial distribution of the vertical elastic displacement caused by each modeled fault segment compared with the MIS 5.5 paleo-shoreline elevation trend;

Figure 8b. Fault modeling results for T2, T3, T5, T6.

Figure 8c. Sections 1 and 2: fault modeling results for T7 and T8, respectively. Sections 3 and 4: fault-induced uplift estimates along the STF1 for terraces T1 and T0, respectively.

Figure 9. Quantitative estimates of regional and local uplift rates along the Pollino-Castrovillari (PCF), Satanasso (STF1) and Valsinni (VF1) faults.

Figure 10. Time-partitioned local vertical displacement rates related to the STF1 and VF1 faults.

Table 1. Main morphologic and sedimentary parameters of the T0-T9 marine terraces. Coastal sectors where higher uplift rates are suggested by an increase in inner margin elevations and in altimetric difference between successive marine terraces are in bold.

Table 2. Modified after *Santoro et al*. [2009]. Mean values of the nominal inner margin elevations along the Pollino Range and the Sibari and San Nicola plains derive from observed morphological

inner margins corrected for erosive phenomena, continental cover and paleo-bathymetry of sea-level markers.

Table 3. MIS 5.5 coastal marker data along the northern Taranto Gulf [*Ferranti et al.*, 2006], the southern San Nicola Plain (this work) and the Sila Massif [*Santoro et al.*, 2009].

Table 4. Geometric and kinematics parameters of the modeled fault segments, obtained through iterative comparison between paleo-shorelines shape and vertical displacement models. Bracket values indicate the range of possible values extracted from seismic reflection profile F75-89. Slip rate (mm/a) are referred to the last 400 ka and were evaluated only for the fault segments that deform the terraces (STF1and VF1). The Mw is derived from scalar relationships of *Wells and Coppersmith* [1994] (see the text for further details).

Table 5. Parametric information of the Pollino-Castrovillari fault (from the DISS database: http://diss.rm.ingv.it/diss/).

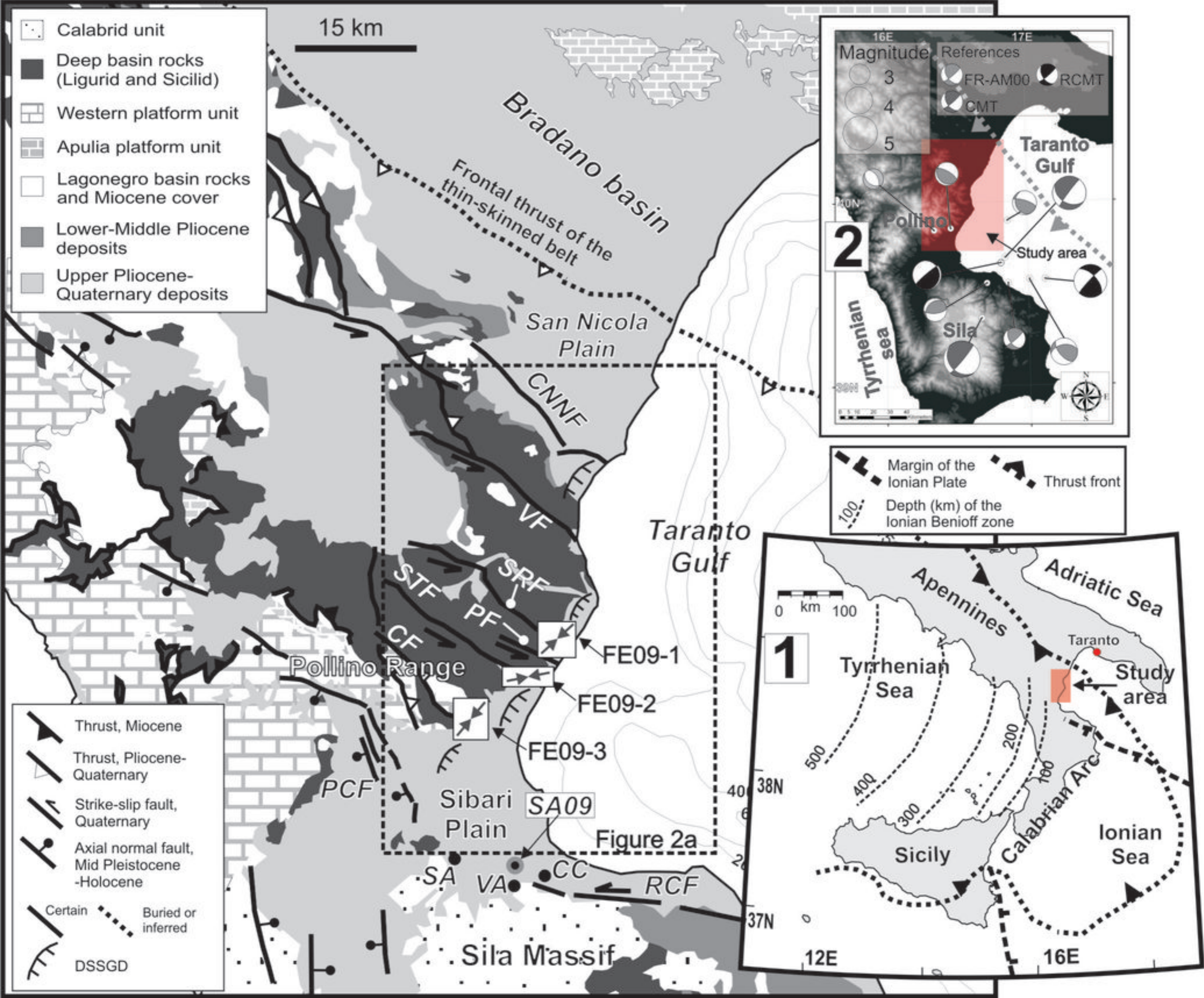
Calabrid unit
Deep basin rocks (Ligurid and Sicilid)
Western platform unit
Apulia platform unit
Lagonegro basin rocks and Miocene cover
Lower-Middle Pliocene deposits
Upper Pliocene-Quaternary deposits
15 km
Bradano basin
Frontal thrust of the thin-skinned belt
San Nicola Plain
CNNF
VF
SRF
STF
PF
CF
FE09-1
FE09-2
FE09-3
Pollino Range
Taranto Gulf
PCF
Sibari Plain
SA09
Figure 2a
SA
VA
CC
RCF
Sila Massif
Thrust, Miocene
Thrust, Pliocene-Quaternary
Strike-slip fault, Quaternary
Axial normal fault, Mid Pleistocene-Holocene
Certain
Buried or inferred
DSSGD
16E
17E
Magnitude
3
4
5
References
FR-AM00
RCMT
CMT
Taranto Gulf
Pollino
Study area
2
Tyrrhenian sea
Sila
40N
39N
Margin of the Ionian Plate
Thrust front
Depth (km) of the Ionian Benioff zone
100
0
km
100
1
Tyrrhenian Sea
Apennines
Adriatic Sea
Taranto
Study area
500
400
300
200
100
Calabrian Arc
Sicily
Ionian Sea
38N
37N
12E
16E
400
200

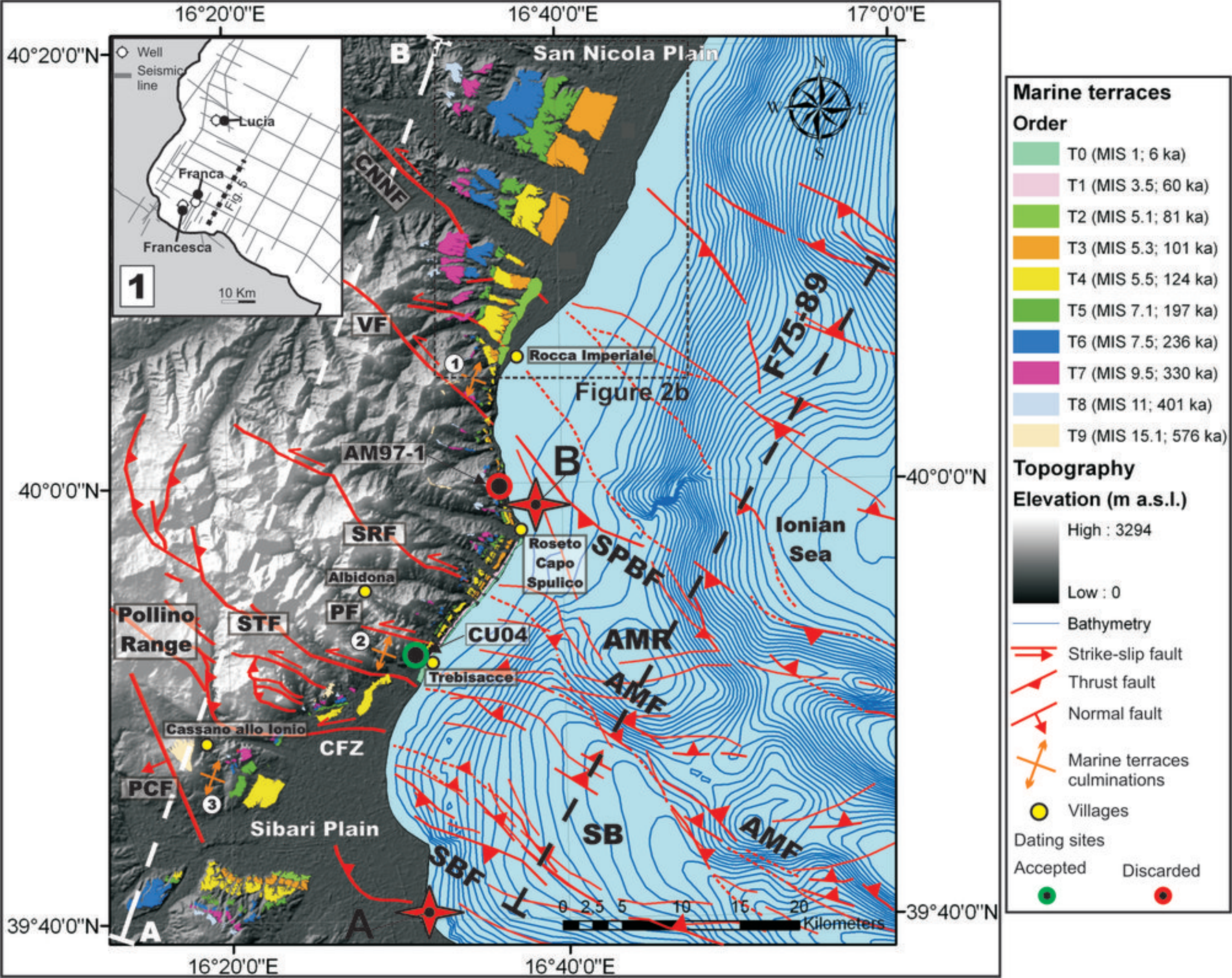
16°20'0"E
16°40'0"E
17°0'0"E
40°20'0"N
40°0'0"N
39°40'0"N
Well
Seismic line
Lucia
Franca
Francesca
Fig. 5
1
10 Km
B
San Nicola Plain
N
S
W
E
CNNF
VF
①
Rocca Imperiale
Figure 2b
F75-89
AM97-1
B
SRF
Roseto Capo Spulico
SPBF
Ionian Sea
Albidona
PF
Pollino Range
STF
②
CU04
Trebisacce
AMR
AMF
Cassano allo Ionio
CFZ
PCF
③
Sibari Plain
SB
AMF
SBF
A
A
0 2.5 5 10 15 20 Kilometers
Marine terraces
Order
T0 (MIS 1; 6 ka)
T1 (MIS 3.5; 60 ka)
T2 (MIS 5.1; 81 ka)
T3 (MIS 5.3; 101 ka)
T4 (MIS 5.5; 124 ka)
T5 (MIS 7.1; 197 ka)
T6 (MIS 7.5; 236 ka)
T7 (MIS 9.5; 330 ka)
T8 (MIS 11; 401 ka)
T9 (MIS 15.1; 576 ka)
Topography
Elevation (m a.s.l.)
High : 3294
Low : 0
Bathymetry
Strike-slip fault
Thrust fault
Normal fault
Marine terraces culminations
Villages
Dating sites
Accepted
Discarded

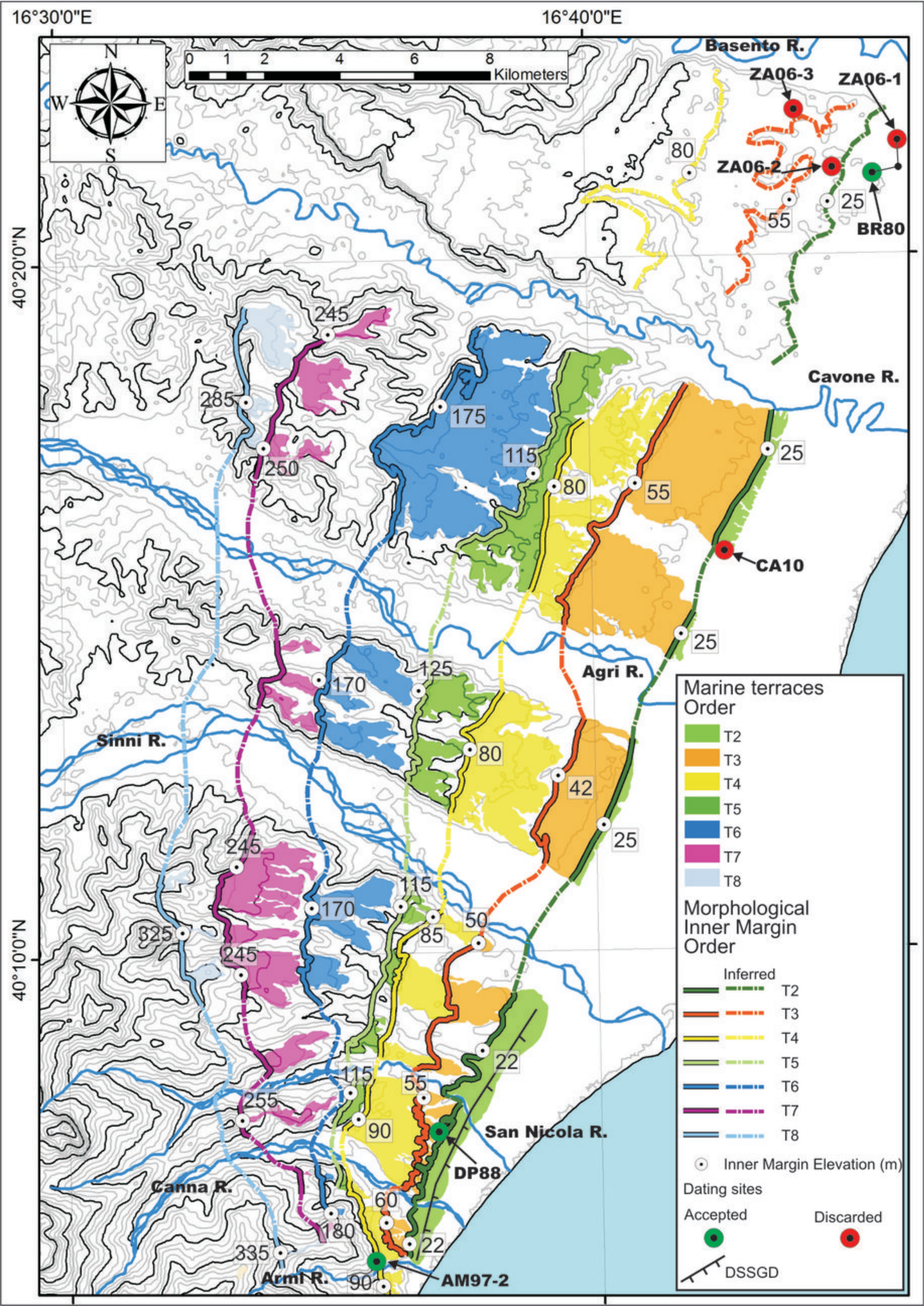
16°30'0"E
16°40'0"E
40°20'0"N
40°10'0"N
N
S
W
E
0
1
2
4
6
8
Kilometers
Basento R.
Cavone R.
Agri R.
Sinni R.
San Nicola R.
Canna R.
Armi R.
ZA06-3
ZA06-1
ZA06-2
BR80
CA10
DP88
AM97-2
80
55
25
245
285
250
175
115
80
55
25
25
125
170
80
42
25
245
115
170
85
50
325
245
22
115
55
255
90
60
180
22
335
90
Marine terraces Order
T2
T3
T4
T5
T6
T7
T8
Morphological Inner Margin Order
Inferred
T2
T3
T4
T5
T6
T7
T8
Inner Margin Elevation (m)
Dating sites
Accepted
Discarded
DSSGD

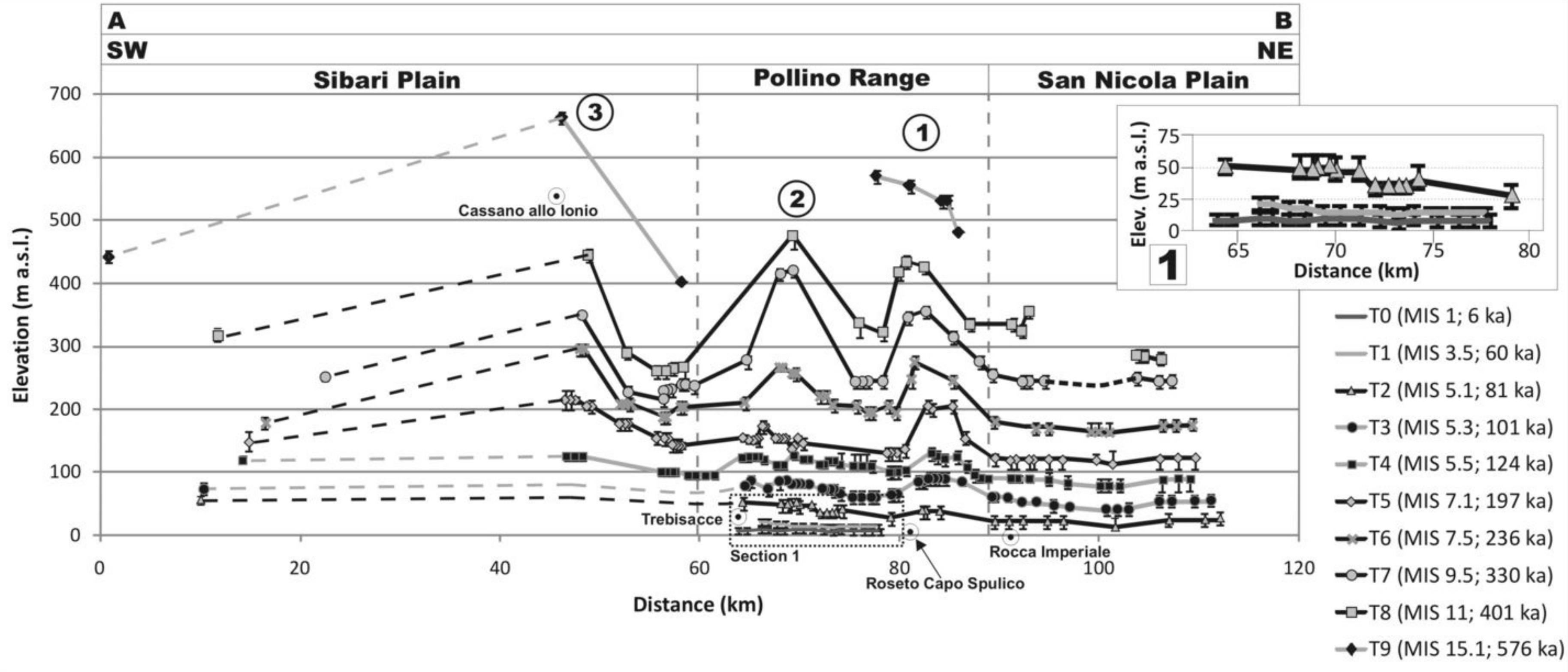
A
B
SW
NE
Sibari Plain
Pollino Range
San Nicola Plain
Elevation (m a.s.l.)
700
600
500
400
300
200
100
0
Distance (km)
0
20
40
60
80
100
120
③
②
①
Cassano allo Ionio
Trebisacce
Section 1
Roseto Capo Spulico
Rocca Imperiale
Elev. (m a.s.l.)
75
50
25
0
65
70
75
80
Distance (km)
1
T0 (MIS 1; 6 ka)
T1 (MIS 3.5; 60 ka)
T2 (MIS 5.1; 81 ka)
T3 (MIS 5.3; 101 ka)
T4 (MIS 5.5; 124 ka)
T5 (MIS 7.1; 197 ka)
T6 (MIS 7.5; 236 ka)
T7 (MIS 9.5; 330 ka)
T8 (MIS 11; 401 ka)
T9 (MIS 15.1; 576 ka)

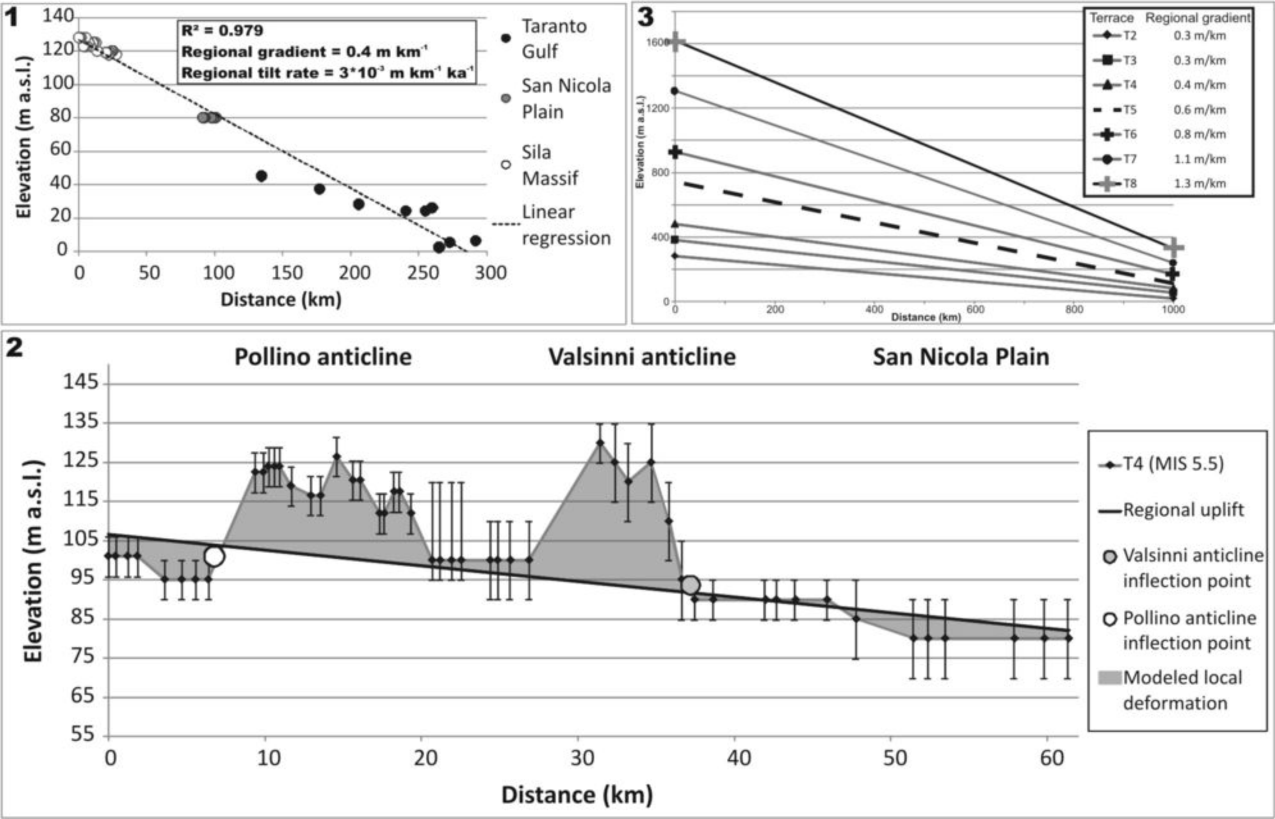
1
R² = 0.979
Regional gradient = 0.4 m km⁻¹
Regional tilt rate = 3*10⁻³ m km⁻¹ ka⁻¹
Elevation (m a.s.l.)
Distance (km)
0
20
40
60
80
100
120
140
0
50
100
150
200
250
300
Taranto Gulf
San Nicola Plain
Sila Massif
Linear regression
3
Terrace
Regional gradient
T2
0.3 m/km
T3
0.3 m/km
T4
0.4 m/km
T5
0.6 m/km
T6
0.8 m/km
T7
1.1 m/km
T8
1.3 m/km
Elevation (m a.s.l.)
Distance (km)
0
400
800
1200
1600
0
200
400
600
800
1000
2
Pollino anticline
Valsinni anticline
San Nicola Plain
Elevation (m a.s.l.)
Distance (km)
55
65
75
85
95
105
115
125
135
145
0
10
20
30
40
50
60
T4 (MIS 5.5)
Regional uplift
Valsinni anticline inflection point
Pollino anticline inflection point
Modeled local deformation

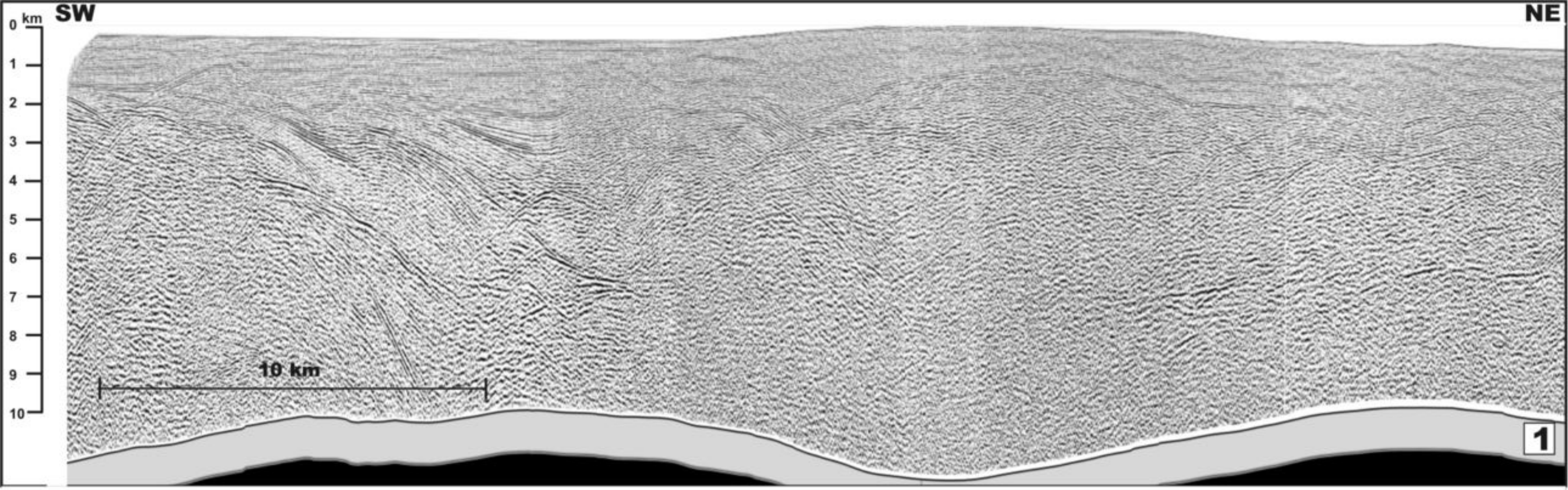
SW
NE
0 km
1
2
3
4
5
6
7
8
9
10
10 km
1

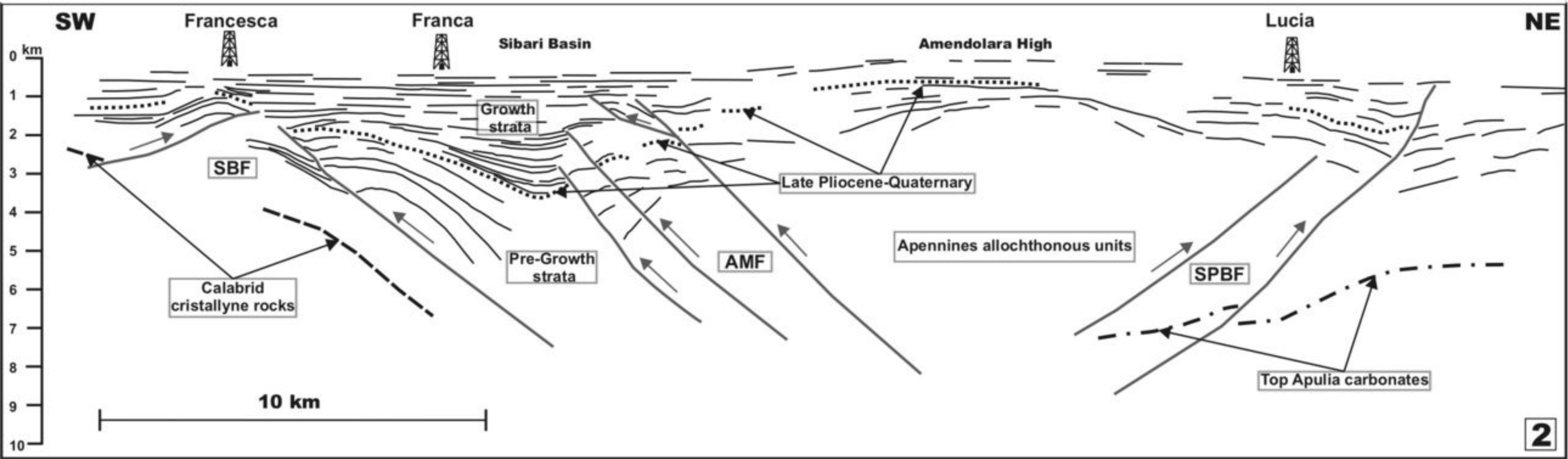
SW
Francesca
Franca
Sibari Basin
Amendolara High
Lucia
NE
0 km
1
2
3
4
5
6
7
8
9
10
Growth strata
SBF
Late Pliocene-Quaternary
Apennines allochthonous units
Pre-Growth strata
AMF
SPBF
Calabrid cristallyne rocks
Top Apulia carbonates
10 km
2

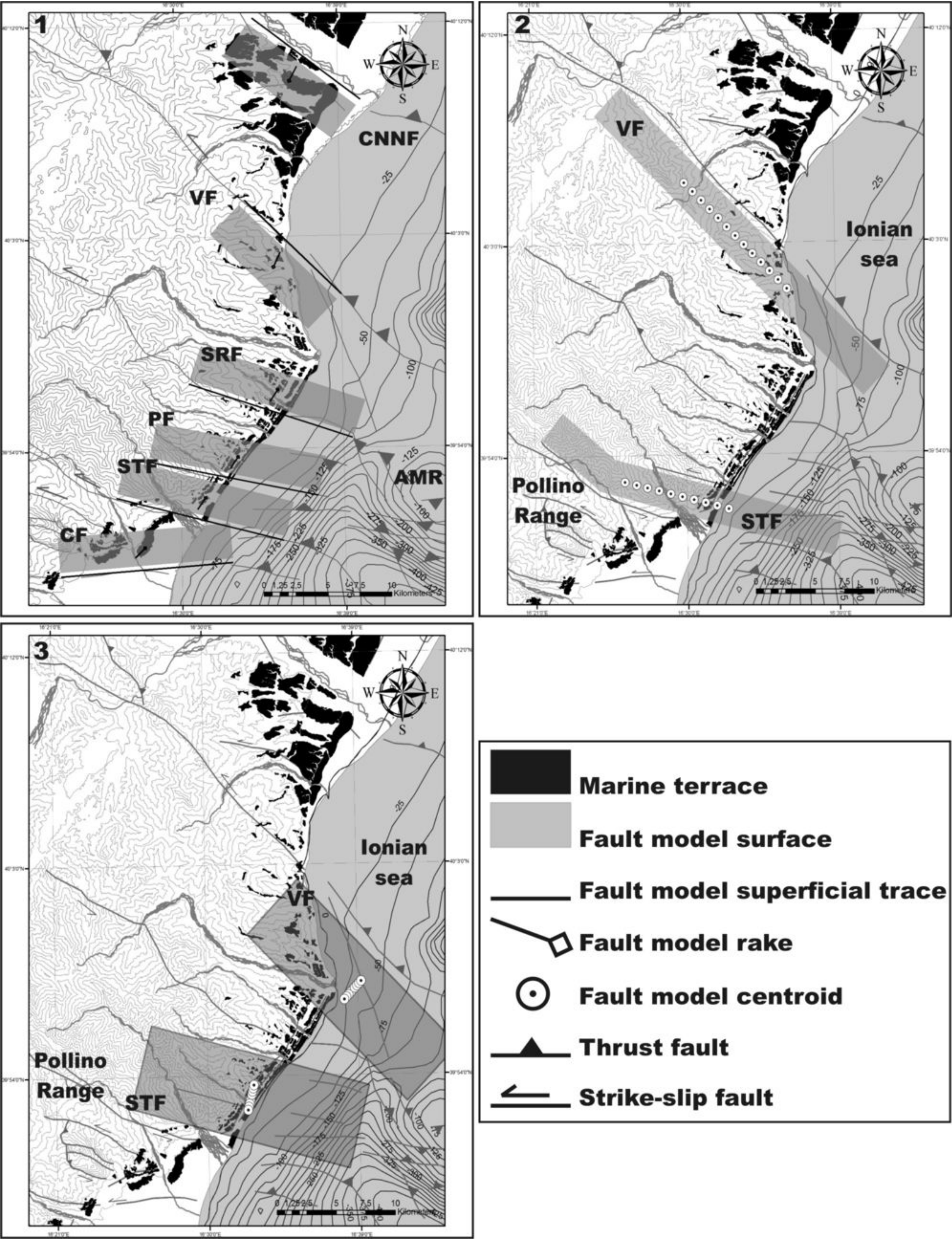
1
CNNF
VF
SRF
PF
STF
CF
AMR
2
VF
Ionian sea
Pollino Range
STF
3
Ionian sea
VF
Pollino Range
STF
N
S
W
E
0 1,25 2,5 5 7,5 10 Kilometers
-25
-50
-75
-100
-125
-150
-175
-200
-225
-250
-275
-300
-325
-350
-375
-400
-425
40°12'0"N
40°3'0"N
39°54'0"N
16°21'0"E
16°30'0"E
16°39'0"E
Marine terrace
Fault model surface
Fault model superficial trace
Fault model rake
Fault model centroid
Thrust fault
Strike-slip fault

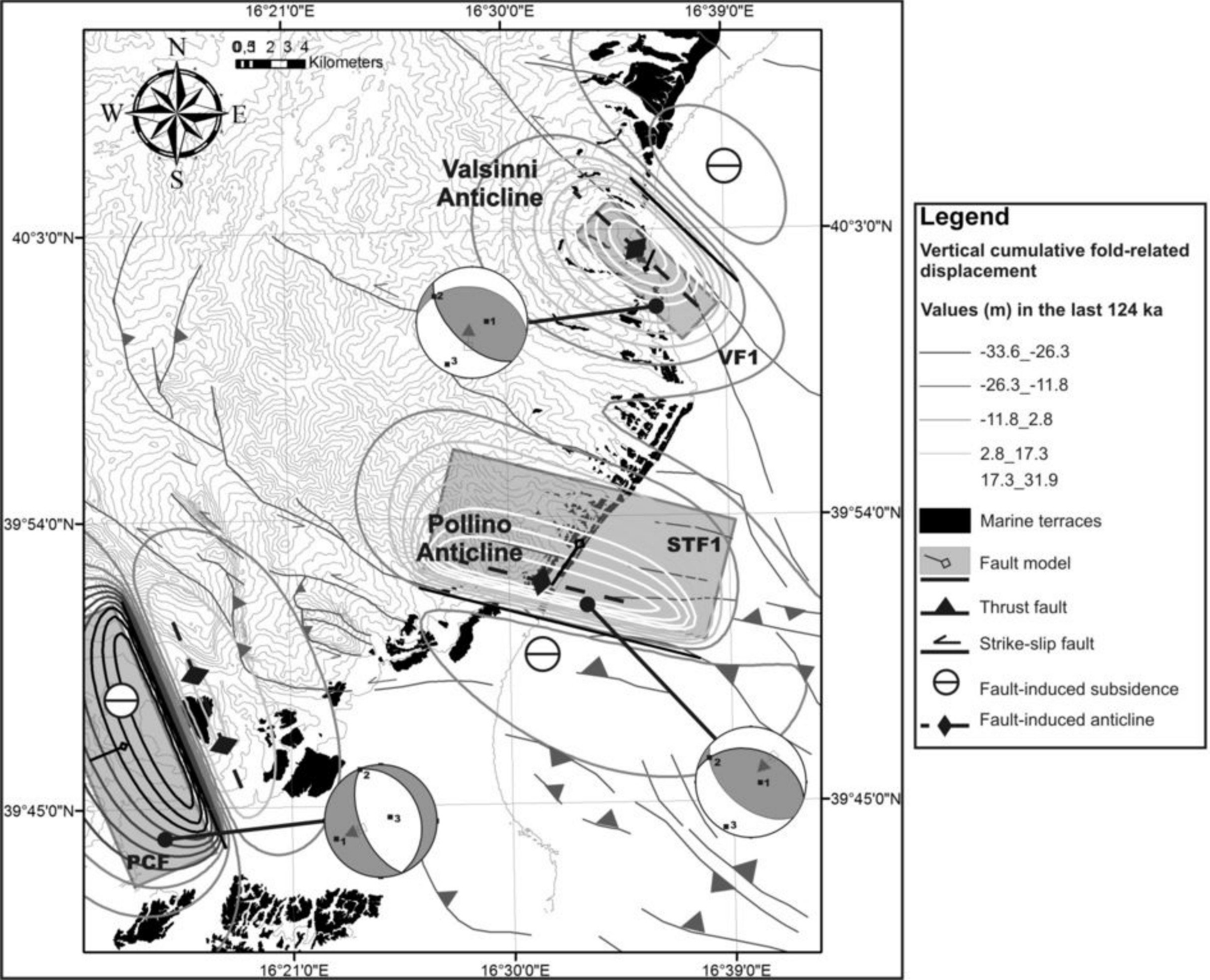
16°21'0"E
16°30'0"E
16°39'0"E
40°3'0"N
39°54'0"N
39°45'0"N
N
S
W
E
0,5 1 2 3 4
Kilometers
Valsinni Anticline
Pollino Anticline
VF1
STF1
PCF
1
2
3
Legend
Vertical cumulative fold-related displacement
Values (m) in the last 124 ka
-33.6_-26.3
-26.3_-11.8
-11.8_2.8
2.8_17.3
17.3_31.9
Marine terraces
Fault model
Thrust fault
Strike-slip fault
Fault-induced subsidence
Fault-induced anticline

1

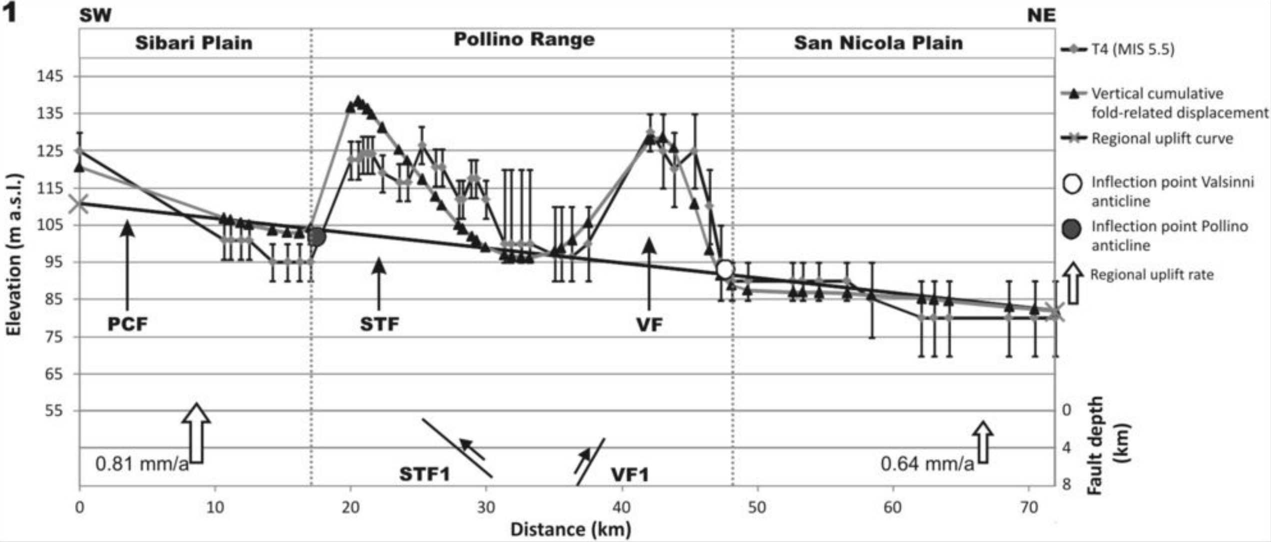
SW
NE
Sibari Plain
Pollino Range
San Nicola Plain
T4 (MIS 5.5)
Vertical cumulative fold-related displacement
Regional uplift curve
Inflection point Valsinni anticline
Inflection point Pollino anticline
Regional uplift rate
PCF
STF
VF
0.81 mm/a
0.64 mm/a
STF1
VF1
Elevation (m a.s.l.)
145
135
125
115
105
95
85
75
65
55
Fault depth (km)
0
4
8
Distance (km)
0
10
20
30
40
50
60
70

2

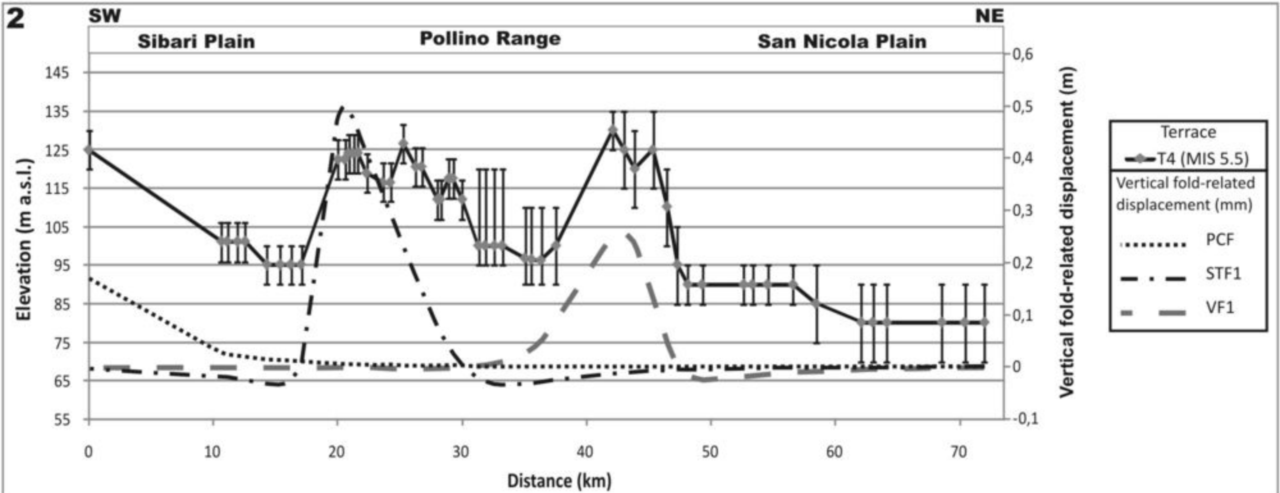
SW
NE
Sibari Plain
Pollino Range
San Nicola Plain
Elevation (m a.s.l.)
145
135
125
115
105
95
85
75
65
55
Vertical fold-related displacement (m)
0,6
0,5
0,4
0,3
0,2
0,1
0
-0,1
Terrace
T4 (MIS 5.5)
Vertical fold-related displacement (mm)
PCF
STF1
VF1
Distance (km)
0
10
20
30
40
50
60
70

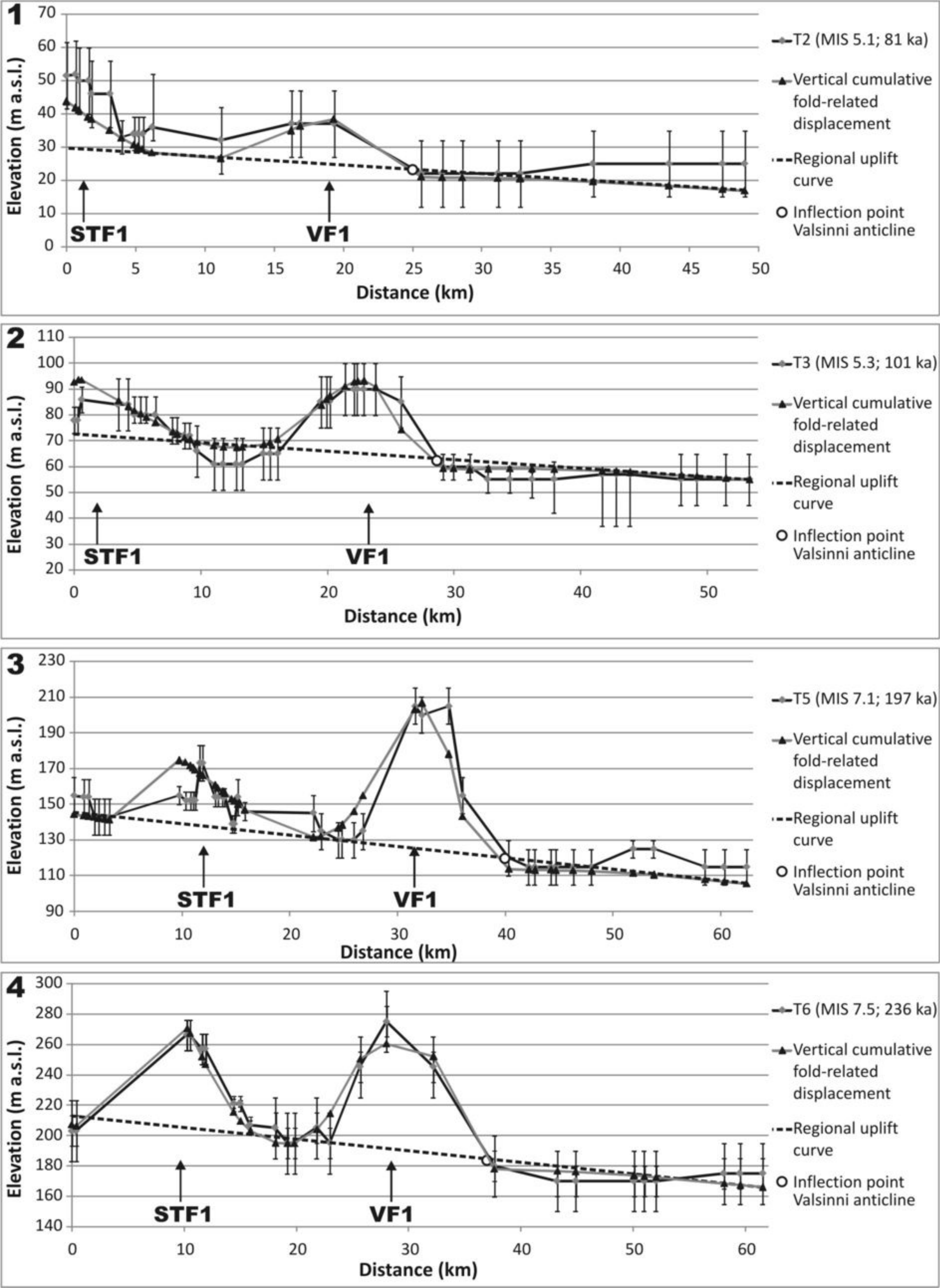
1
Elevation (m a.s.l.)
70
60
50
40
30
20
10
0
STF1
VF1
0
5
10
15
20
25
30
35
40
45
50
Distance (km)
T2 (MIS 5.1; 81 ka)
Vertical cumulative fold-related displacement
Regional uplift curve
Inflection point Valsinni anticline
2
Elevation (m a.s.l.)
110
100
90
80
70
60
50
40
30
20
STF1
VF1
0
10
20
30
40
50
Distance (km)
T3 (MIS 5.3; 101 ka)
Vertical cumulative fold-related displacement
Regional uplift curve
Inflection point Valsinni anticline
3
Elevation (m a.s.l.)
230
210
190
170
150
130
110
90
STF1
VF1
0
10
20
30
40
50
60
Distance (km)
T5 (MIS 7.1; 197 ka)
Vertical cumulative fold-related displacement
Regional uplift curve
Inflection point Valsinni anticline
4
Elevation (m a.s.l.)
300
280
260
240
220
200
180
160
140
STF1
VF1
0
10
20
30
40
50
60
Distance (km)
T6 (MIS 7.5; 236 ka)
Vertical cumulative fold-related displacement
Regional uplift curve
Inflection point Valsinni anticline

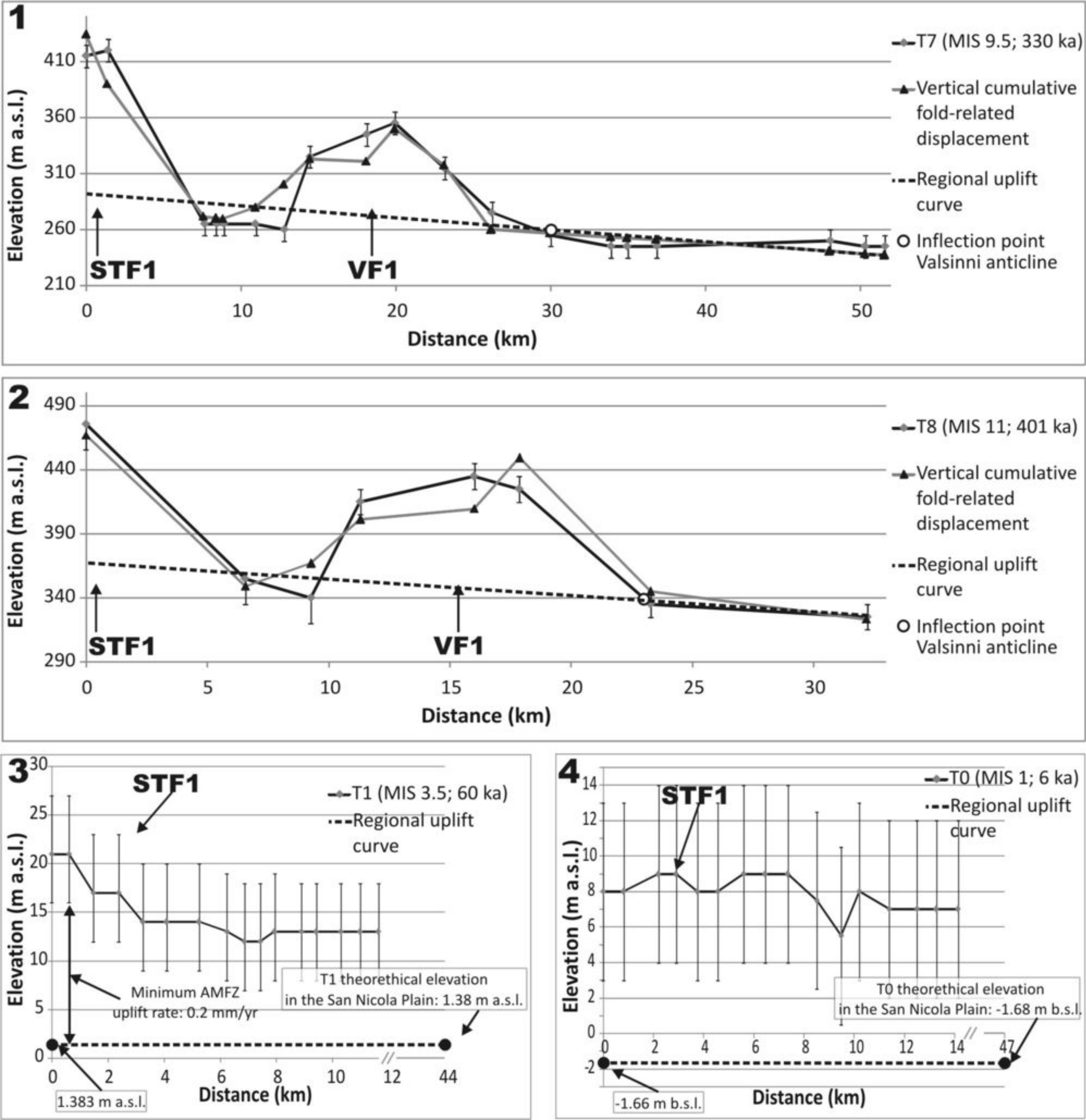
1
Elevation (m a.s.l.)
410
360
310
260
210
0
10
20
30
40
50
Distance (km)
STF1
VF1
T7 (MIS 9.5; 330 ka)
Vertical cumulative fold-related displacement
Regional uplift curve
○ Inflection point Valsinni anticline
2
Elevation (m a.s.l.)
490
440
390
340
290
0
5
10
15
20
25
30
Distance (km)
STF1
VF1
T8 (MIS 11; 401 ka)
Vertical cumulative fold-related displacement
Regional uplift curve
○ Inflection point Valsinni anticline
3
Elevation (m a.s.l.)
30
25
20
15
10
5
0
0
2
4
6
8
10
12
44
Distance (km)
STF1
T1 (MIS 3.5; 60 ka)
Regional uplift curve
Minimum AMFZ uplift rate: 0.2 mm/yr
T1 theorethical elevation in the San Nicola Plain: 1.38 m a.s.l.
1.383 m a.s.l.
4
Elevation (m a.s.l.)
14
12
10
8
6
4
2
0
-2
0
2
4
6
8
10
12
14
47
Distance (km)
STF1
T0 (MIS 1; 6 ka)
Regional uplift curve
T0 theorethical elevation in the San Nicola Plain: -1.68 m b.s.l.
-1.66 m b.s.l.

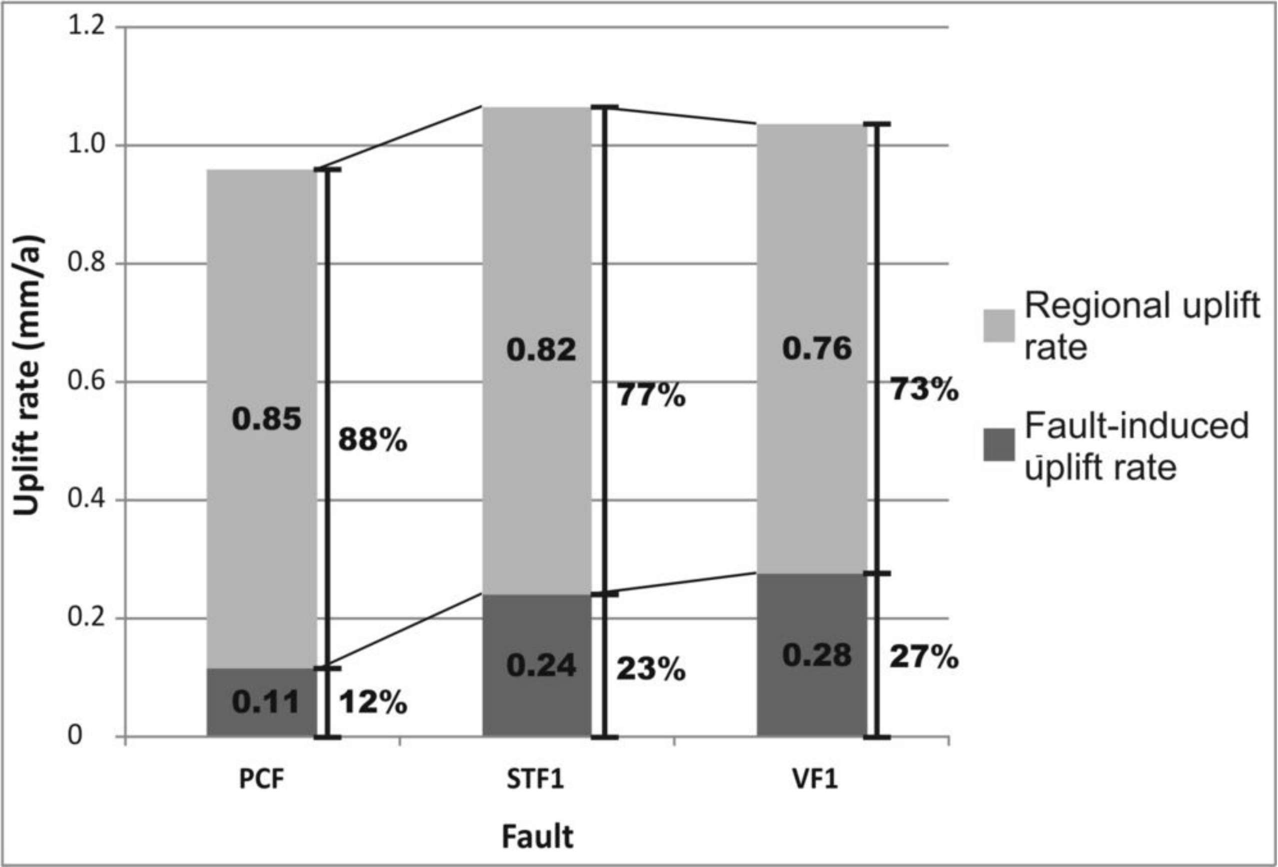
Uplift rate (mm/a)
1.2
1.0
0.8
0.6
0.4
0.2
0
0.85
88%
0.11
12%
0.82
77%
0.24
23%
0.76
73%
0.28
27%
PCF
STF1
VF1
Fault
Regional uplift rate
Fault-induced uplift rate

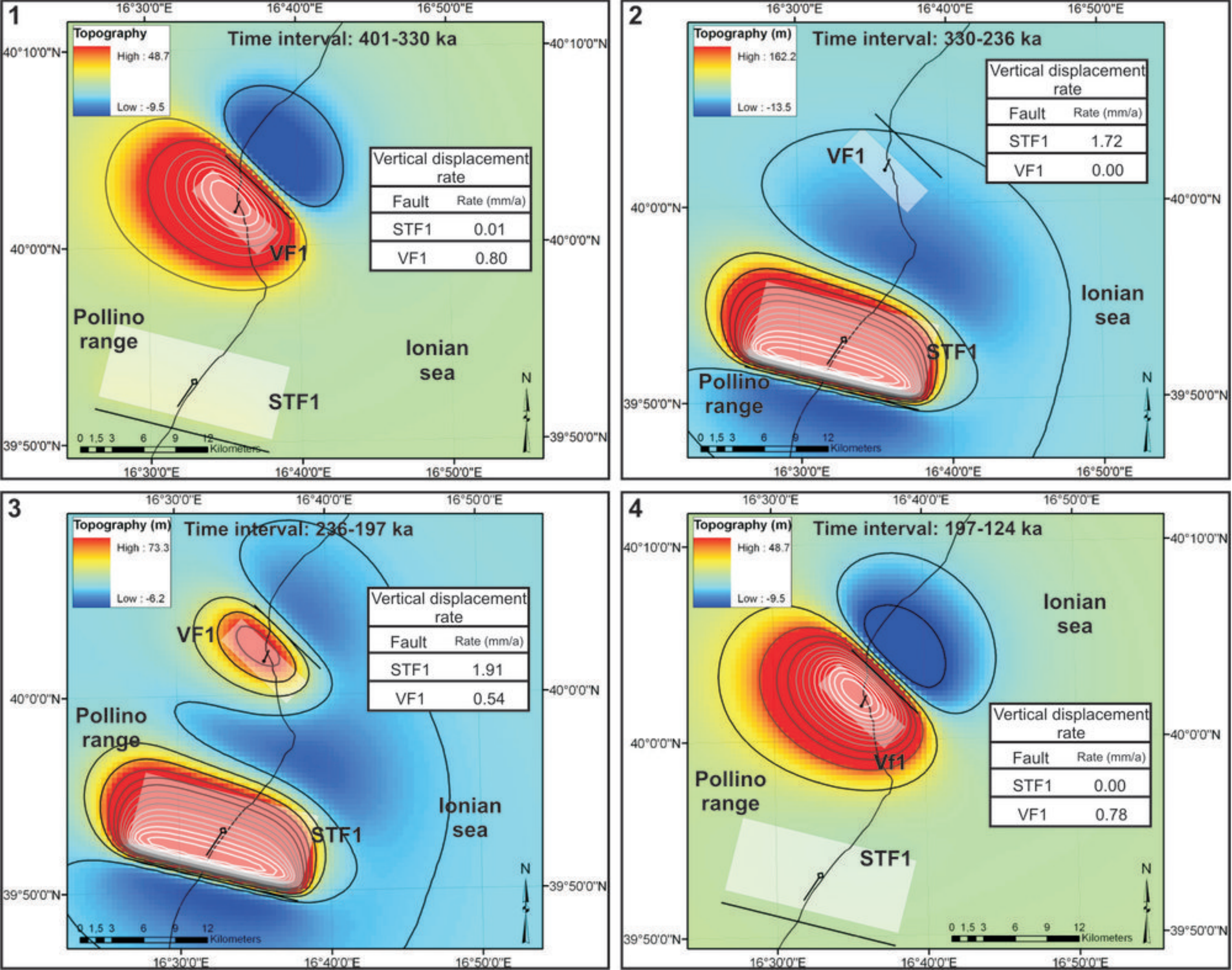

Vertical displacement rate

Fault	Rate (mm/a)
STF1	0.01
VF1	0.80

Vertical displacement rate

Fault	Rate (mm/a)
STF1	1.72
VF1	0.00

Vertical displacement rate

Fault	Rate (mm/a)
STF1	1.91
VF1	0.54

Vertical displacement rate

Fault	Rate (mm/a)
STF1	0.00
VF1	0.78

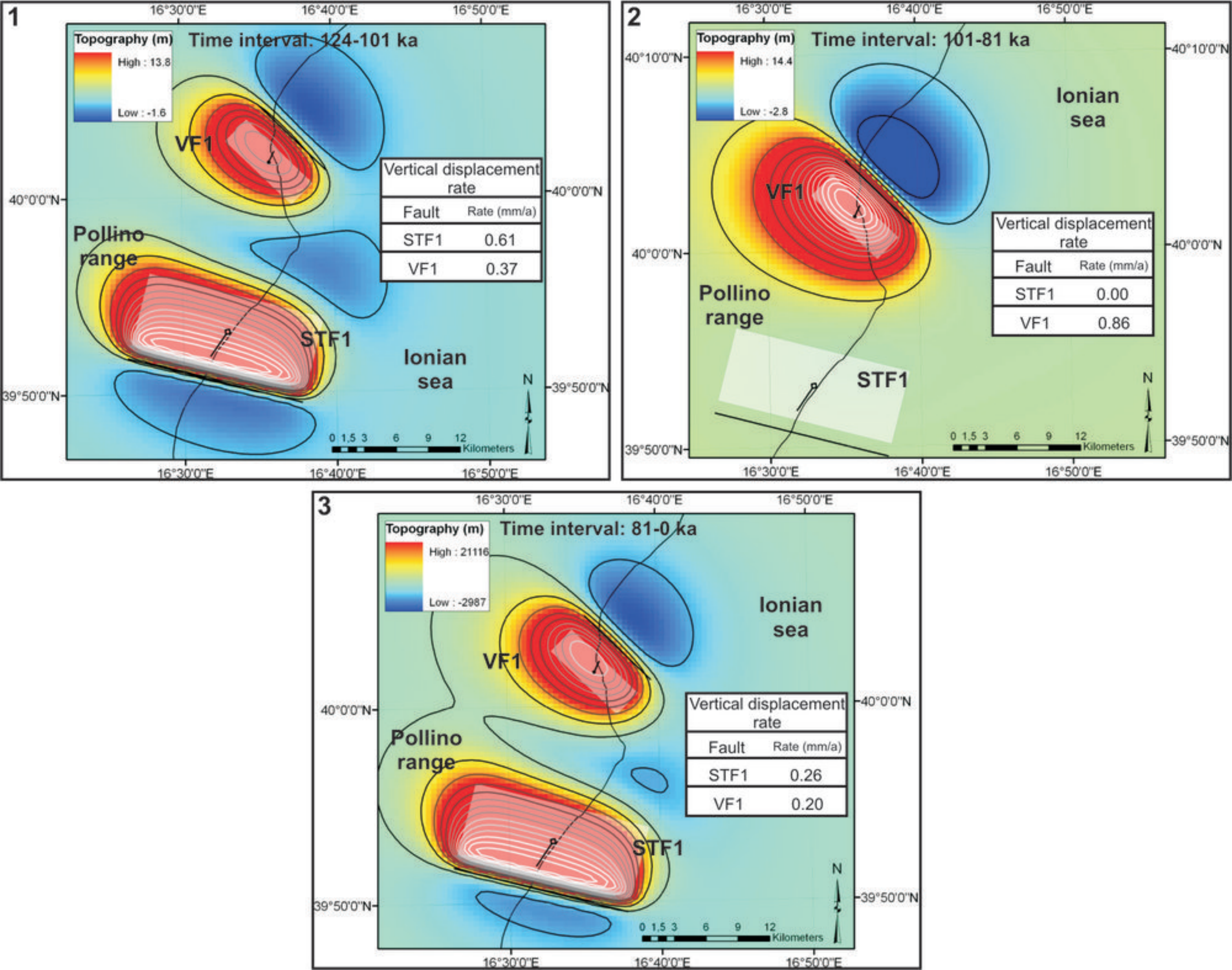
1
Topography (m)
High : 13.8
Low : -1.6
Time interval: 124-101 ka
VF1
Pollino range
STF1
Ionian sea
Vertical displacement rate
Fault | Rate (mm/a)
STF1 | 0.61
VF1 | 0.37
16°30'0"E
16°40'0"E
16°50'0"E
40°0'0"N
39°50'0"N
N
0 1,5 3 6 9 12 Kilometers
2
Topography (m)
High : 14.4
Low : -2.8
Time interval: 101-81 ka
Ionian sea
VF1
Pollino range
STF1
Vertical displacement rate
Fault | Rate (mm/a)
STF1 | 0.00
VF1 | 0.86
16°30'0"E
16°40'0"E
16°50'0"E
40°10'0"N
40°0'0"N
39°50'0"N
N
0 1,5 3 6 9 12 Kilometers
3
Topography (m)
High : 21116
Low : -2987
Time interval: 81-0 ka
Ionian sea
VF1
Pollino range
STF1
Vertical displacement rate
Fault | Rate (mm/a)
STF1 | 0.26
VF1 | 0.20
16°30'0"E
16°40'0"E
16°50'0"E
40°0'0"N
39°50'0"N
N
0 1,5 3 6 9 12 Kilometers

Terrace	Inner Margin altimetric range (m)			Average width (m)				Average slope (degree)			Platform - Cliff ratio				Maximum deposit thickness (m)			Altimetric range between successive marine terrace orders (m) [b]			
	PSN	PLL	SB	PSN	PLL	SB	Tot	PSN	PLL	SB	PSN	PLL	SB	Tot	PSN	PLL	SB				
T0	X	**5.5-9**	X	X	204	X	204	X	1.1	X	X	30.5	X	30.5	X	X	X	Terrace	PSN	PLL	SB
T1	X	**12-21**	X	X	211	X	211	X	1.2	X	X	8.4	X	8.4	X	9[a]	X	T0-T1	X	7	X
T2	22-25	**22-51**	X	999	99	X	549	0.7	5.6	X	35.7	2.7	X	19.2	X	13	X	T1-T2	X	25	X
T3	42-60	**60-90**	X	2849	235	X	1542	0.5	3.4	X	86.3	6.2	X	46.3	X	11	X	T2-T3	28	**36**	X
T4	80-90	**90-130**	95-125	2035	358	1516	1303	1.0	3.1	1.2	63.1	8.8	21.9	31.3	8	45	>25	T3-T4	33	**38**	X
T5	115	120-205	**143-215**	893	266	489	549	1.5	4.0	2.0	15.4	4.1	7.5	9.0	20	23	50	T4-T5	32	41	**69**
T6	170-175	180-275	**187-295**	1538	415	320	757	1.3	2.6	2.1	43.9	7.7	9.2	20.3	2	13	23	T5-T6	58	**65**	**65**
T7	245-250	**240-355**	215-350	1639	532	387	852	1.6	3.0	2.9	25.5	5.5	10.9	14.0	X	X	25	T6-T7	35	**54**	35
T8	275-355	**303-435**	260-445	969	686	273	643	1.3	3.5	2.8	X	4.9	1.2	3.1	X	X	>8	T7-T8	64	**97**	35
T9	X	470-570	**400-663**	X	796	1397	1097	X	2.9	2.9	X	X	X	X	X	X	X	T8-T9	X	141	**234**

PSN = San Nicola Plain

PLL = Pollino Range

SB = Sibari Plain

Tot = Total study area

[a] Well data

[b] Calculated between pairs of inner margins

Terrace	Nominal inner margin mean elevation (m a.s.l.)			MIS	Age (Ka)	Paleo-sea level (m)	Reference	Uplift (m)			Time partitioned uplift rate (mm/a)			Markers couplets[a]		
	Sibari Plain	Pollino Range	San Nicola Plain					Sibari Plain	Pollino Range	San Nicola Plain	Sibari Plain	Pollino Range	San Nicola Plain	Sibari Plain	Pollino Range	San Nicola Plain
T0	X	8	X	1	5.9	-5.3	*Lambeck et al.* [2011]	X	13	X	X	2.2	X	X	T0/Sea level	X
T1	X	15	X	3.5	60.5	-35.7	*Waelbroeck et al.* [2002]	X	50	X	X	0.7	X	X	T1/T0	X
T2	X	40	24	5.1	81.5	-31.0		X	71	55	X	1.0	0.7	X	T2/T1	T2/Sea level
T3	X	76	51	5.3	101	-12.9		X	89	64	X	0.9	0.5	X	T3/T2	T3/T2
T4	105	114	85	5.5	123.9	6.3		99	108	78	0.8	0.8	0.6	T4/Sea level	T4/T3	T4/T3
T5	175	155	117	7.1	197	-9.7		184	164	126	1.2	0.8	0.7	T5/T4	T5/T4	T5/T4
T6	227	227	172	7.5	236	0.3		227	227	172	1.1	1.6	1.2	T6/T5	T6/T5	T6/T5
T7	262	281	246	9.5	330.5	-5.0		267	286	251	0.7	0.7	0.8	T7/T6	T7/T6	T7/T6
T8	298	378	310	11	401	6.5		291	372	304	0.8	1.2	0.7	T8/T7	T8/T7	T8/T7
T9	532	519	X	15.1	576.4	-9.2	*Lisiecki and Raymo* [2005]	541	529	X	1.4	0.9	X	T9/T8	T9/T8	X

---

[a] Sequential markers couplets for calculation of the time partitioned uplift rates.

Locality	Coastal sector	Long	Lat	Coastal marker	Vertical uncertainty (m)	Shoreline elevation (m a.s.l.)	Uplift rate (mm/a)	Faunal assemblage	Dating tecnique	Age (Ka)	Reference(s)
Castellaneta - Ponte del Re	NTG	16.947	40.52	Inner margin	20	45	0.31	*Persististrombus latus*	Paleontology, Aminostrtigraphy	X	*Boenzi et al.* [1985]; *Caldara* [1988]; *Dai Pra and Hearty* [1988]; *Hearty and Dai Pra* [1992]
Taranto - Ponte Romano	NTG	17.172	40.53	Inner margin	20	37	0.25	*Cladocora Caespitosa*	U-Th	107.7±1.5	*Mastronuzzi and Sansò* [2003]
Masseria Santa Teresiola	NTG	17.257	40.508	Beach deposits	5	28	0.18	*Persististrombus latus, Cladocora Caespitosa*	Paleontology, U-Th	125±6; 205±20; 162+23/-18; 89.8±4.8; 93+8.8/-8.1	*Dai Pra and Stearns* [1977]; *Hearty and Dai Pra* [1992]; *Mastronuzzi and Sansò* [2003]
Masseria Tuglia - Masseria Pantaleo	NTG	17.292	40.468	Beach deposits	3	24	0.14	*Persististrombus latus, fauna senegalensis*	Paleontology	X	*Dai Pra and Stearns* [1977]; *Mastronuzzi* [2001]; *Mastronuzzi and Sansò* [2003]
Masseria Abete Resta	NTG	17.274	40.425	Beach deposits	3	24	0.14	*Persististrombus latus*	Paleontology	X	*Mastronuzzi and Sansò* [2003]
Lizzano - Canale dei Lupi	NTG	17.432	40.377	Beach deposits	3	26	0.16	*Persististrombus latus*	Paleontology	X	*Cotecchia et al.* [1971]; *Hearty and Dai Pra* [1992]
Torre Castiglione	NTG	17.82	40.288	Beach deposits	3	2	-0.03	*Persististrombus latus*	Paleontology, U-Th	156±20	*Dai Pra and Stearns* [1977]; *Dai Pra* [1982]; *Hearty and Dai Pra* [1992]
Gallipoli	NTG	17.996	40.065	Beach deposits	3	5	-0.01	*Persististrombus latus*	Aminostrtigraphy	X	*Cotecchia et al.* [1971]; *Hearty and Dai Pra* [1985]; *Hearty and Dai Pra* [1992]
Grotta del Diavolo/Capo Santa Maria di Leuca	NTG	18.347	39.792	Beach deposits - speleothems	2	6	0	X	Morphostratigraphical correlation	X	*Mastronuzzi and Sansò* [2003]

Recoleta	SNP	16,655	40,278	Inner margin	20	80	0:59	X	Morphostratigraphical correlation	X	This work
Masseria Mostazzo	SNP	16,627	40,215	Inner margin	15	80	0:59	X	Morphostratigraphical correlation	X	This work
Masseria Pantanello	SNP	16,603	40,161	Inner margin	15	90	0.68	X	Morphostratigraphical correlation	X	This work
Masseria Leuci	SNP	16,591	40,127	Inner margin	10	90	0.68	X	Morphostratigraphical correlation	X	This work
Spezzano Albanese	SM	16,307	39,694	Inner margin	15	120	0.92	X	Morphostratigraphical correlation	X	*Santoro et al.* [2009]
Vaccarizzo Albanese	SM	16,462	39,628	Inner margin	20	123	0.94	X	Electron Spin Resonance	135±20	*Santoro et al.* [2009]
Rossano Calabro	SM	16,641	39,586	Inner margin	15	125	0.96	X	Morphostratigraphical correlation	X	*Santoro et al.* [2009]
Rossano (Fossa)	SM	16,726	39,584	Inner margin	20	130	1	X	Morphostratigraphical correlation	X	*Santoro et al.* [2009]

NTG = northern Taranto Gulf
SNP = San Nicola Plain
SM = Sila Massif

Onland Fault	Offshore Fault	Fault segment	Centroid coordinates		Strike	Plunge	Dip	Rake	Co-seismic slip (m)	Length (km)	Width (km)	Area (km^2)	Minimum depth (km)	Maximum depth (km)	Slip rate (mm/a)	Mw
			Longitude	Latitude												
PF	AMF	PF1	16.5662	39.916	282	12	48(+10/-20)	68	1	19	10.1	191.9	1(+2)	8.5 (-2.5/+0.5)	0.5	6.4
STF		STF1	16.5483	39.8857	285	15	40(+20/-10)	70	1	16.9	9.3	157.2	1(+2)	7(-1/+2)		6.3
SRF		SRF1	16.4745	40.0119	308	38	48(+10/-20)	25	1	19	10.1	191.9	1(+2)	8.5(-2.5/+0.5)		6.4
VF	SPBF	VF1	16.5967	40.0291	135	225	60 (-30)	110	1	8.7	5.8	50.5	3(-2)	8 (-2/+1)	0.7	5.9

AMF = Amendolara Fault
PF = Pagliara Fault
SPBF = Spulico Basin Fault
SRF = Saraceno Fault
STF = Satanasso Fault
VF = Valsinni Fault

Parametric information		Source type	Source
Location (Lat/Lon; ED50)	39.7841/16.237	LD	Based on geological data from *Cinti et al.* [1995].
Length (km)	15.6	LD	Based on geological data from *Cinti et al.* [1995].
Width (km)	10.3	ER	Calculated using the scalar relationships from W*ells and Coppersmith* [1994].
Minimum depth (km)	1	LD	Based on geological data from *Cinti et al.* [1995].
Maximum depth (km)	9.9	AR	Derived from dip, width and minimum depth.
Strike (degree)	158	LD	Based on geological data from *Cinti et al.* [1995].
Dip (degree)	60	LD	Based on geological data from *Cinti et al.* [1995].
Rake (degree)	270	LD	Based on geological and seismotectonic informations.
Slip per event (m)	0.8 - 1.6	LD	Based on paleoseismological data from *Cinti et al.* [1997].
Slip rate (mm/a)	0.2 - 0.6	LD	Based on geological data and markers dislocation.
Vertical slip rate (mm/a)	0.2 - 0.5	LD	Based on geological observations of displaced markers.
Recurrence time (yr)	1170	LD	Based on paleoseismological data from *Cinti et al.* [1997].
Magnitude (Mw)	6.2	ER	Calculated using the scalar relationships from W*ells and Coppersmith* [1994].

LD = literature data

ER = empirical relationship

AR = analytical relationship